Journal Pre-proofs

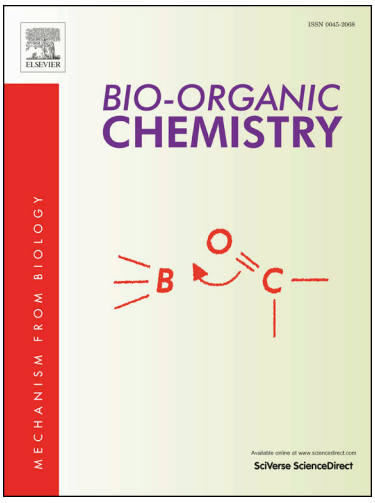

Novel Pyrazine Based Anti-tubercular Agents: Design, Synthesis, Biological Evaluation and *In Silico* Studies

Nayera W. Hassan, Manal N. Saudi, Yasser S. Abdel-Ghany, Azza Ismail, Perihan A. Elzahhar, Dharmarajan Sriram, Rasha Nassra, Marwa M. Abdel-Aziz, Soad A. El-Hawash

PII: S0045-2068(19)31273-8
DOI: https://doi.org/10.1016/j.bioorg.2020.103610
Reference: YBIOO 103610

To appear in: *Bioorganic Chemistry*

Received Date: 4 August 2019
Revised Date: 2 December 2019
Accepted Date: 20 January 2020

Please cite this article as: N.W. Hassan, M.N. Saudi, Y.S. Abdel-Ghany, A. Ismail, P.A. Elzahhar, D. Sriram, R. Nassra, M.M. Abdel-Aziz, S.A. El-Hawash, Novel Pyrazine Based Anti-tubercular Agents: Design, Synthesis, Biological Evaluation and *In Silico* Studies, *Bioorganic Chemistry* (2020), doi: https://doi.org/10.1016/j.bioorg.2020.103610

Novel Pyrazine Based Anti-tubercular Agents: Design, Synthesis, Biological Evaluation and *In Silico* Studies

Nayera W. Hassan[1], Manal N. Saudi[1], Yasser S. Abdel-Ghany[1], Azza Ismail[1], Perihan A. Elzahhar[1], Dharmarajan Sriram[2], Rasha Nassra[3], Marwa M. Abdel-Aziz[4], Soad A. El-Hawash[1*]

[1]Department of Pharmaceutical Chemistry, Faculty of Pharmacy, Alexandria University, Alexandria 21521, Egypt.

[2]Medicinal Chemistry and Drug Discovery Research Laboratory, Pharmacy Group, Birla Institute of Technology and Science-Pilani, Hyderabad Campus, Jawahar Nagar, Telangana 500078, India

[3]Department of Medical Biochemistry, Faculty of Medicine, Alexandria University, Alexandria, Egypt.

[4]The Regional Center for Mycology and Biotechnology, Al-Azhar University, Cairo 11759, Egypt.

ABSTRACT

TB continues to be a leading health threat despite the availability of powerful anti-TB drugs. We report herein the design and synthesis of various hybrid molecules comprising pyrazine scaffold and various formerly identified anti-mycobacterial moieties. Thirty-one compounds were screened *in vitro* for their activity against Mycobacterium Tuberculosis H_{37}Rv strain using MABA assay. The results revealed that six compounds **(8a, 8b, 8c, 8d, 14b** and **18)** displayed significant activity against *Mtb* with MIC values ≤ 6.25 µg/ml versus 6.25 µg/ml for pyrazinamide. The most active compounds were then assessed for their *in vitro* cytotoxicity against PBMC normal cell line using MTT assay and showed SI > 200. Several *in silico* studies have been carried out for target fishing of the novel compounds such as shape-based similarity, pharmacophore mapping and inverse docking. Based on this multi-step target fishing study, we suggest that pantothenate synthetase could be the possible target responsible for the action of these compounds. The most active compounds were then successfully docked into the active site of

pantothenate synthetase enzyme with favorable binding interactions. In addition, *in silico* prediction of physicochemical, ADMET and drug-like properties were also determined indicating that compounds **8b, 8c** and **8d** are promising candidates for the development of new anti-TB agents with enhanced activity and better safety profile.

Keywords: Antimycobacterial evaluation; Pyrazine analogs; Hydrazide/hydrazones; Target fishing; Inverse docking; Drug-likeness.

***Corresponding Authors:**

Soad A. El-Hawash, *Department of Pharmaceutical Chemistry, Faculty of Pharmacy, Alexandria University, Alexandria, Egypt.*

Email: Soad.elhawash@alexu.edu.eg
Soadhawash@yahoo.com

1. Introduction

Tuberculosis (TB) is one of the most fatal infectious diseases caused by the bacillus *Mycobacterium tuberculosis* (*Mtb*) [1]. It has been and still remains a high priority public health threat throughout the world, significantly in developing nations [2]. According to the latest World Health Organization (WHO) report, it is an ailment affecting approximately 10 million people each year and is enlisted among the top causes of death worldwide [3]. For the past five years, it preceded HIV/AIDS and has been the principal reason for death from a sole infectious agent [3]. The spread of drug-resistant TB (DR-TB) is a global ill health problem that hinders the success of TB management programs. The emergence of multidrug-resistant tuberculosis (MDR-TB) and extensively drug-resistant TB (XDR-TB) has exacerbated the global TB scenario substantially [4]. Nowadays, the standard chemotherapy recommended by the WHO comprises 2 months of intensive, directly observed treatment (DOT) with four first-line drugs isoniazid (INH), rifampin (RIF), pyrazinamide (PZA) and ethambutol (EMB), followed by a minimum of 4 months of INH and RIF. MDR-TB necessitates a further 2 years of treatment with combination therapy including three of second-line drugs, such as quinolones, aminoglycosides, D-cycloserine in addition to any first-line drug to which the isolate is susceptible [1, 5]. The success of the prevailing anti-TB drugs enticed the general view that TB could be effectively held in reserve and even eradicated. In spite of half a century of anti-TB therapy, one-third of the world's population asymptomatically still harbor a dormant or latent form of *Mtb* with a lifetime risk of disease reactivation [6]. Therefore, a key challenge facing the anti-TB drug discovery is identifying new drugs with good sterilizing activity that can eliminate 'persisters', remaining after the growing bacteria have been abolished by bactericidal agents [7]. The obstinate nature of persistent infection and upsurge in MDR-TB and XDR-TB are the main challenges for effective treatment of TB with many of the currently existing anti-TB drugs [8].

Thus, there is an imperative need for finding new anti-TB drugs with enhanced properties such as better activity against DR strains, less toxicity, shorter duration of therapy and prompt mycobactericidal mechanism of action [9].

PZA is a critical first-line drug for TB treatment as it constitutes, along with INH and RIF, the keystone of contemporary TB therapy [10]. It plays a unique role in reducing therapy duration from 9–12 months to 6 months. This is because, in conjunction with RIF, PZA is the solitary active drug to retain the so-called sterilizing activity as it kills a population of dormant non-growing tubercle bacilli of low metabolic activity in acidic pH environments. Other anti-TB drugs lose their activity under these acidic conditions [11, 12]. In spite of PZA utilization in clinical practice since the 1950s, its complex mechanism of action remains inapprehensible among the anti-TB drugs [13]. Many efforts have been attempted to elucidate the exact mechanism of action behind the sterilizing effect of PZA. Conversion of PZA to pyrazinoic acid (POA) could play the key role in its action, since PZA-resistant strains lack the enzyme responsible for the conversion to POA (namely pyrazinamidase, PZase) [14, 15]. Based chiefly on biochemical clues, several separate proteins were proposed to be targeted by POA. POA was suggested to inhibit fatty acid synthesis via fatty acid synthase-I (FAS-I) [16] and trans-translation, a process that releases ribosomes paused during translation, by interaction with ribosomal protein S1/RpsA [17]. However, queries have been raised regarding these suggested mechanisms [18, 19]. As well, it was hypothesized that POA, a structural analog of quinolinic acid, suppreses the catalytic activity of quinolinic acid phosphoribosyl transferase (QAPRTase) and, hence, de novo NAD biosynthesis [20]. POA was also suggested to bind to aspartate decarboxylase (PanD) triggering its degradation by Mtb, thus blocking biosynthesis of the crucial bacterial Coenzyme A [21]. Recently, it was found that extremely high concentrations (mM) of POA could inhibit guanosine pentaphosphate synthase (GpsI) which is implicated in nucleic acid and guanosine pentaphosphate (ppGpp) metabolism [22]. Nonetheless, many reports disproved the previously stated mechanisms of action [23-27].

In addition, the pyrazine ring manifested its status in the field of antimycobacterial agents [28-32]. Numerous active anti-tubercular agents containing pyrazinamide nucleus are frequently encountered in literature. These agents either contained a linker -such as the carbohydrazide (**A**) or chalcone (**B**) linker or were directly attached (**C**) to various aromatic/heterocyclic rings; as shown in **Figure 1**.

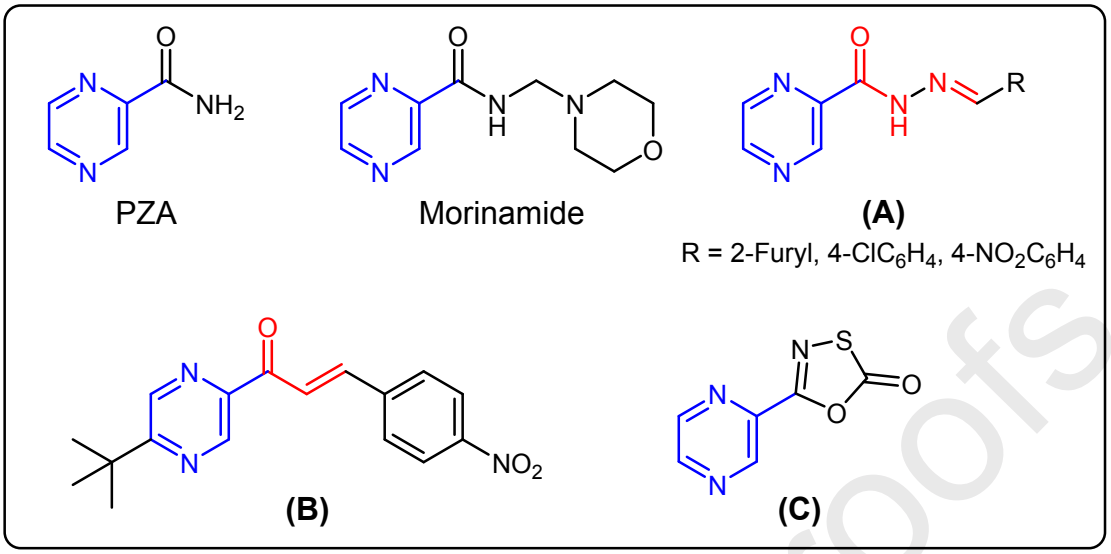

Figure 1. Reported pyrazine based anti-tubercular agents

Based on the aforementioned facts, the present work illustrates the synthesis of a series of compounds by introducing carbohydrazide linker to afford pyrazine-2-carbohydrazide derivatives (**6a-c**, **8a-d**). This selection was based on the fact that many anti-TB hydrazones act as prodrugs [33-35]. In addition, further structural modification of the carbohydrazide linker has been proposed by inverting the linker such that the carbonyl group is directly attached to the bioactive heterocyclic moiety rather than the pyrazine ring (**10**, **11**, **12a-e**) to evaluate the influence of the different linkers on the biological activity against *Mtb*.

Furthermore, in an effort to decrease the flexibility of the linker, the carbohydrazide function was incorporated into a ring structure (**13a-e**) to investigate the effect of such structural modification on the anticipated biological activity. Additionally, pyrazine bearing chalcones have been also proposed (**14a,b**) owing to their widely-recognized anti-TB activity since 1950's [36]. Moreover, a series of hybrid molecules was designed by directly attaching the pyrazine ring with various bioactive heterocyclic moieties (**15-24**) to investigate their anti-TB activity and the necessity of linkers for the activity. The selected heterocyclic moieties (pyrazoline, isoxazole, pyrimidine and dihydropyridine) have attracted continuing interest and were found to be promising anti-TB structural units [37-40]. Finally, in a trial to investigate the effect of hetero atom on the anticipated biological

activity, a representative carbocyclic analog (**25**) was synthesized to evaluate its anti-TB effect (**Figure 2**).

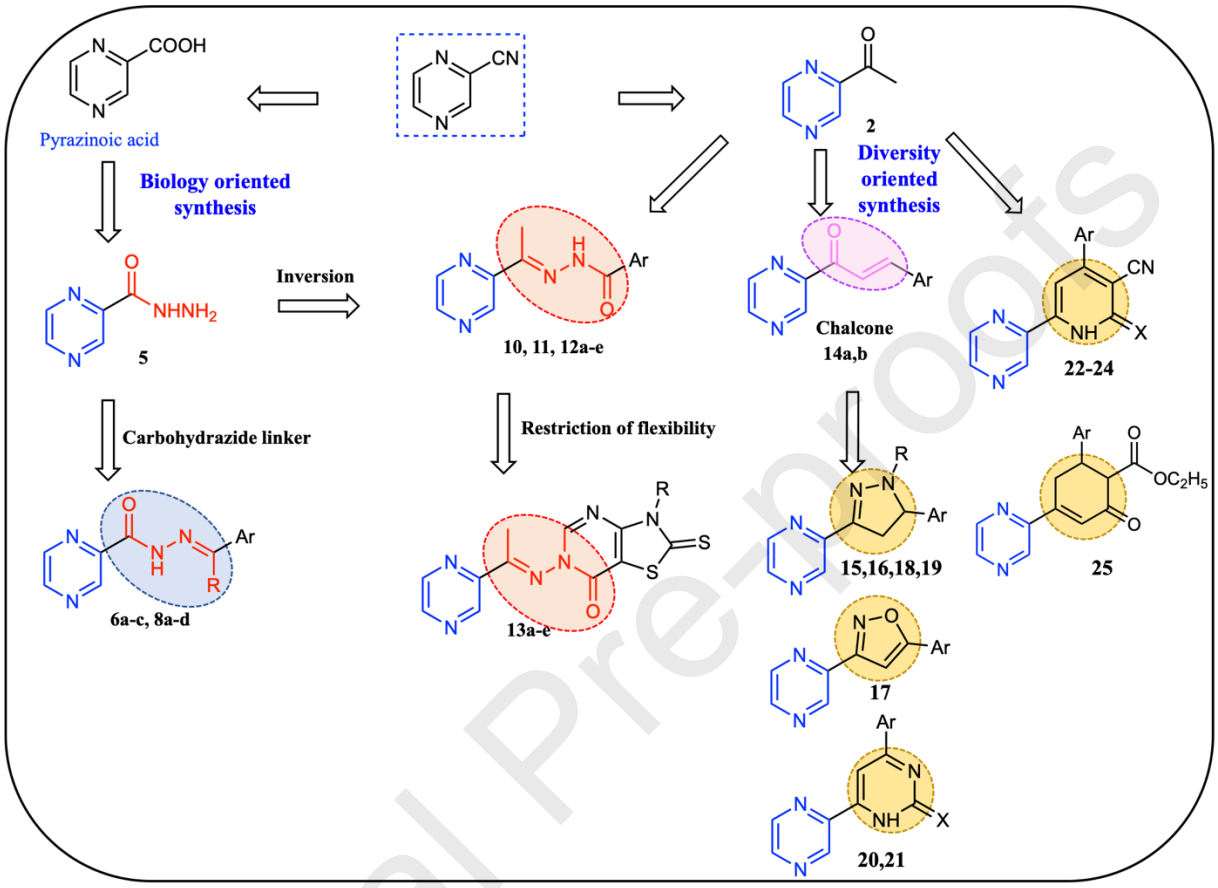

Figure 2. Outline for the design of the target compounds.

It is noteworthy mentioning that an interesting and fruitful approach for exploring biologically relevant space to develop new bioactive molecules is "Biology-oriented synthesis or **BIOS**". It entails efficient building on existing clinically-useful agents to generate novel bioactive compounds with enhanced biological activities [41]. We employed this approach for the synthesis of the target hydrazones **6** and **8**, reckoning on pyrazinoic acid, the active form of pyrazinamide (PZA) (**Figure 2**). On the other hand, a diversity-guided strategy, known as diversity-oriented synthesis or **DOS**, was engaged in order to attain high level of functional and structural versatility that can increase the chances of finding molecules with exciting biological characters [42]. This was productively achieved via using a simple starting material such as acetyl pyrazine, that

was converted into a set of structurally diversified pyrazine derivatives (**10-25**) in few synthetic steps as depicted in **Figure 2**.

The present work is therefore directed towards the design and synthesis of various novel pyrazine scaffold containing compounds to evaluate their anti-TB activity. Cytotoxicity assay, physicochemical and pharmacokinetic parameters were also performed. A target fishing study is carried out to elucidate the possible mechanism of action.

2. Results and Discussion

2.1. Chemistry

The synthetic routes adopted for the preparation of the target compounds are outlined in **Schemes 1-4.**

The starting material, 2-acetyl pyrazine (**2)** was prepared from pyrazine-2-carbonitrile via Grignard reaction according to reported procedures [43, 44].

Scheme 1 describes the preparation of the intermediate pyrazine-2-carboxylic acid hydrazide (**5)** through alkaline hydrolysis of pyrazine-2-carbonitrile (**1)** to obtain pyrazine-2-carboxylic acid (**3)** followed by esterification and hydrazinolysis to give **5** in a good yield. The target hydrazones **6a-c** and **8a-d** were prepared by the condensation of the hydrazide **5** with the appropriate ketones or pyrazole aldehydes (**7a-d)** in ethanol according to the procedure described in literature [45]. The ^{1}H-NMR spectra for compounds **6a-c** showed one characteristic upfield singlet corresponding to methyl protons at δ 2.42-2.57 ppm and a D_2O exchangeable singlet corresponding to NH proton at δ 11.15-11.24 ppm. The latter values coincided with reported chemical shifts of NH for similar compounds of 9-12 ppm for the *E*-isomer [46]. Interestingly, spectrum of compound **6a** displayed additional D_2O exchangeable singlet corresponding to OH at δ 15.39 ppm. This could be attributed to the existence of amide-iminol tautomerism at a ratio 1:2 which indicated that iminol tautomer was the predominant one. The careful inspection of the ^{1}H-NMR spectra of compounds **8a-d** indicated the stereoselectivity of the condensation step as depicted by the presence of only one imino-hydrogen (N=CH) signal for each N-acylhydrazone derivative at higher chemical shifts at δ 8.80-8.93 ppm, which was attributed to the (*E*)-stereoisomer [47].

In **scheme 2**, the key intermediate cyanoacetic acid hydrazide **9** was prepared by condensing **2** with cyanoacetic acid hydrazide in boiling absolute ethanol, applying the reported reaction conditions of related compounds [48]. The target 2-imino-2*H*-chromene-3-carbohydrazide derivative **10** was obtained by reacting **9** with salicylaldehyde in presence of piperidine as a catalyst. Acidic hydrolysis of **10** afforded the corresponding 2-oxo-2*H*-chromene-3-carbohydrazide derivative **11**. The ^{1}H-NMR spectrum of **9** showed one D_2O exchangeable signal assigned for deshielded NH proton at δ 11.34 ppm in addition to an upfield singlet assigned for methylene protons at δ 4.33 ppm, while that of **10** revealed the disappearance of the methylene protons and showed an extra D_2O exchangeable signal due to the imino proton at δ 9.33 ppm. The ^{1}H-NMR spectrum of **11** lacked the signal for =NH present in the precursor and its IR spectrum displayed an absorption band characteristic to lactone C=O at 1700 cm^{-1}. Gewald reaction of compound **9** yielded the target compounds **12a-e,** which then underwent cyclization in a mixture of triethylorthoformate and acetic anhydride to give **13a-e**. The ^{1}H-NMR spectra for **12a-e** exhibited a broad D_2O exchangeable singlet at δ 7.36-8.02 ppm, corresponding to NH_2 protons. The ^{1}H-NMR spectra for **13a-e** lacked signals for NH and NH_2 protons and indicated a characteristic singlet at δ 8.54-8.71 ppm corresponding to –CH=N proton.

Scheme 3 illustrates the synthesis of the target chalcones **14a**, **b** via the condensation of **2** with aromatic aldehydes. ^{1}H-NMR spectrum of compound **14a,b** revealed characteristic signals for olefinic protons in the range of δ 6.93-8.14 ppm. Interestingly, the magnitude of the olefinic vicinal coupling constant between the two protons (*J*=16 Hz) in the^{1}H-NMR spectrum of compound **14b** indicated the existence of the *E* configuration. In addition, the IR spectra of those compounds showed expected shift of C=O stretching frequency to 1661-1662 cm^{-1} due to increased conjugation. Compound **14a** was refluxed with hydrazine hydrate or phenyl hydrazine in ethanol to give the respective pyrazole derivatives **15a**,**b**, while its reaction with hydrazine hydrate in acetic acid afforded the ethanone derivative **16**. Additionally, **14a** was treated with hydroxylamine hydrochloride to give the corresponding isoxazole derivative **17**. Moreover, reaction of **14a** with thiosemicarbazide gave the corresponding carbothioamide derivative **18** which was further reacted with phenacyl bromide to afford phenylthiazole derivative **19**. ^{1}H-NMR spectra of compounds **15a, b, 16, 18** and **19** showed an H_{abx} pattern due to coupling of

the pyrazoline ring protons. The existence of the methylenic protons (H_a and H_b) separately in two peaks, clearly postulated the magnetic non-equivalence of these two protons. ^{1}H-NMR spectrum of **17** lacked the protons' signals of the H_{abx} system and showed a characteristic singlet at δ 6.88 ppm assigned for the isoxazole-C_4-H. It is worth noting that ^{1}H-NMR spectrum of **18** showed two D_2O exchangeable singlets at δ 8.16 ppm and δ 8.26 ppm assigned to the two non-equivalent NH_2 protons which could be attributed to the existence of intra-molecular hydrogen bonding. Furthermore, synthesis of the target compounds **20** and **21**, was achieved by reacting **14a** with urea and thiourea, respectively. ^{1}H-NMR spectrum of **20** displayed two D_2O exchangeable singlets at δ 7.10 and 7.13 ppm assigned for two NH protons which confirmed the presence of the pyrimidinone ring in tautomerized form. ^{1}H-NMR spectrum of **21** showed a characteristic singlet at δ 8.47 ppm assigned for pyrimidine-C_5-H, in addition to two D_2O exchangeable singlets assigned for NH and SH at δ 8.63 and 13.32 ppm, respectively. Other protons' signals characteristic to the molecule appeared as paired signals which confirmed the existence of thione-thiol tautomers at a ratio 2:3.

In **scheme 4**, one pot reaction conditions [49] were adopted to obtain the target compounds **22-25**. Condensation of **2** and the appropriate aromatic aldehyde with malononitrile, ethyl cyanoacetate or cyanothioacetamide in presence of ammonium acetate in ethanol was carried out to afford **22**, **23** and **24**, respectively. Similarly, the cyclohexene carboxylate derivative **25** was obtained by refluxing a mixture of **2**, 3,4-dimethoxybenzaldehyde and ethyl acetoacetate in 10% ethanolic sodium hydroxide. ^{1}H-NMR spectra for compounds **22a,b** revealed one D_2O exchangeable singlet at δ 6.84 and 6.91 ppm assigned for NH_2 protons, respectively. Their IR spectra showed characteristic absorption bands due to C≡N function at 2211 and 2214 cm^{-1} respectively. ^{1}H-NMR spectra of **23a,b** and **24a,b** revealed the appearance of D_2O exchangeable singlet due to NH proton in the range of δ 12.53-13.54 ppm. ^{1}H-NMR spectrum of **25** elicited a characteristic triplet quartet pattern due to the ethyl ester protons.

2.2. Biological Evaluation

2.2.1. Prediction of activity spectra for substances (PASS) analysis

Before performing *in vitro* anti-TB assay, we applied the Prediction of Activity Spectra for Substances (PASS) to explore the biological potential of the synthesized compounds and to prioritize them for further *in vitro* studies. The PASS is an *in silico* tool used for predicting biological activity spectra for natural and synthetic substances, which is based on a robust analysis of structure–activity relationships knowledge base for more than 260 000 compounds with known biological activities including drugs, drug candidates and pharmaceutical leads. The PASS predicts the probable biological potential of the compound based on its structure and reveals the predicted activities as the probability of activity (**Pa**) and inactivity (**Pi**). The higher **Pa** value, the lower is the predicted probability of obtaining false results in biological testing [50, 51]. Predictive anti-TB values for all newly synthesized compounds are summarized in **table 1**. The results obtained revealed that most of the tested compounds exhibited anti-TB activity with **Pa** values in the range of 0.19-0.801. Interestingly, **Pa** values estimated for anti-TB activity for compounds **6b,c** were > 0.7, while compounds **6a, 8a-d, 9, 11, 18** were between 0.5 and 0.7; thus, these compounds could be likely to reveal this activity in *in vitro* assays. PASS analysis of compounds **13b-e**, **16**, **19**, **22b, 23b** and **25** didn't show anti-TB activity, thus compounds **13b,d,e, 16, 19** and **25** were excluded from further *in vitro* biological screening, while compounds **13c, 22b** and **23b** were retained for further biological investigation in order to achieve SAR study. As for the rest of tested compounds, the estimated **Pa** values were found to be in the range of 0.190-0.482. The *in silico* results obtained were further confirmed *in vitro* by MABA assay.

Table 1: Predictive values of anti-TB activity calculated with PASS software

Compound ID	Predicted anti-TB activity	
	Pa	Pi
6a	0.692	0.004
6b	0.767	0.003
6c	0.801	0.003
8a	0.593	0.006
8b	0.660	0.005
8c	0.600	0.006
8d	0.699	0.004
9	0.645	0.005
10	0.432	0.023
11	0.635	0.005
12a	0.461	0.017
12b	0.436	0.022
12c	0.414	0.027
12d	0.347	0.050
12e	0.415	0.027
13a	0.211	0.155
13b	-	-
13c	-	-
13d	-	-
13e	-	-
14a	0.466	0.016
14b	0.211	0.155
15a	0.251	0.118
15b	0.190	0.186
16	-	-
17	0.309	0.067
18	0.592	0.010
19	-	-
20	0.289	0.173
21	0.482	0.014
22a	0.219	0.151
22b	-	-
23a	0.230	0.133
23b	-	-
24a	0.257	0.103
24b	0.190	0.183
25	-	-

2.2.2. *In vitro* anti-mycobacterial assay against $H_{37}RV$

The selected compounds were screened for their *in vitro* activity against *Mtb* $H_{37}Rv$ strain using the microplate alamar blue assay (MABA) [52]. PZA, INH and EMB were used as reference drugs. The results were represented as minimum inhibitory concentration (MIC) values and presented in **table 2**. The tested compounds were found to be effective inhibitors of the growth of *Mtb*. Compounds **8a-d**, **14b** and **18** exhibited promising inhibition with MIC values ≤ 6.25 µg/ml, a value postulated by the global program for the discovery of new anti-TB drugs as an upper threshold for the evaluation of new Mtb therapies [53]. Compound **8b** displayed significant anti-TB activity with MIC value of 0.78 µg/ml which equals two times the activity of EMB (MIC = 1.56 µg/ml) and eight times the activity of PZA (MIC = 6.25 µg/ml). Intriguingly, its MIC value operated within the same order of magnitude as that of the powerful anti-TB reference drug INH, yet, it is still of lower potency. In addition, compounds **8c,d** were found to be as active as EMB and showed four times the activity of PZA. As for compound **8a**, it showed good activity (MIC = 3.12 µg/ml) being two times as active as PZA. Furthermore, compounds **6b,c** and **12c** exhibited moderate anti-*Mtb* activity with MIC value of 12.5 µg/ml which is still comparable to that of PZA. Finally, compounds **6a, 14a** and **23a,b** possessed weak anti-*Mtb* activity with MIC value of 25 µg/ml, showing one fourth the activity of PZA.

Table 2. Anti-mycobacterial activity of the newly synthesized compounds against *Mtb* $H_{37}Rv$ strain (ATCC 27294)

Compound No.	MIC (µg/ml)[a]	CLogP[c]
6a	25	-0.76
6b	**12.5**	**0.19**
6c	**12.5**	**0.19**
8a	**3.12**	**2.17**
8b	**0.78**	**2.89**
8c	**1.56**	**2.51**
8d	**1.56**	**1.85**
9	>25	-0.55
10	>25	0.31
11	>25	0.71
12a	>25	-0.37
12b	>25	0.45
12c	**12.5**	**2.15**
12d	>25	0.55

12e	>25	0.38
13a	>25	-0.17
13c	>25	1.26
14a	25	1.22
14b	**6.25**	**1.22**
15a	>25	1.07
15b	>25	3.03
17	>25	1.52
18	**3.12**	**0.19**
20	>25	1.00
21	>25	1.36
22a	>25	1.53
22b	>25	1.69
23a	25	0.45
23b	25	0.46
24a	>25	0.67
24b	>25	0.68
PZA	**6.25**[b]	**-0.68**
INH	**0.1**	**-0.67**
EMB	**1.56**	**0.12**

[a:] MIC values tested at neutral pH.
[b:] MIC value from testing at pH = 5.6 (acidic) [54].
[c:] LogP (lipophilicity) calculated using "Osiris DataWarrior" software.

2.2.3. Structure Activity Relationship (SAR)

Careful inspection of the structures of the tested compounds revealed that hybrid molecules with carbohydrazide linker between pyrazine and 1,3-diarylpyrazole moieties **(8a-d)** displayed the most potent anti-*Mtb* activity (MIC = 3.12, 0.78, 1.56 and 1.56 µg/ml, respectively). In addition, presence of a substitution at position-4 of phenyl group at pyrazole-C-3 enhanced the activity. The nature of substituents greatly affected the activity (Br > Cl=CH_3). Compound with bromo substituent **(8b)** displayed the highest potency (MIC = 0.78 µg/ml) which might be attributed to the increase of lipophilicity. Replacement of 1,3-diarylpyrazole by pyridinyl or pyrazinyl moieties **(6a-c)** decreased the activity (MIC = 24.26, 12.48 and 12.48 µg/ml, respectively). Moreover, compounds **10, 11, 12a, b, d, e** did not show considerable activity. This clearly revealed that inversion of the carbohydrazide linker was an unfavorable structural modification. However, compound **12c** showed moderate anti-TB activity (MIC = 12.5 µg/ml). This might be attributed to the presence of lipophilic chloro substituent at the phenyl ring of the

dihydrothiazole moiety. Restricting the linker flexibility by incorporation into a ring structure **(13c)** greatly decreased the anti-TB activity (MIC = >25 µg/ml). Furthermore, hybridization between pyrazine and thiophene moiety through three atoms linker resulted in compound **14b** which displayed good anti-TB activity (MIC = 6.25 µg/ml), while hybridization with 3,4-dimethoxyphenyl moiety resulted in compound **14a** with weak activity. This indicated the importance of the heteroatom on the anticipated biological activity. On the other hand, direct attachment of pyrazine with various bioactive heterocycles (compounds **15, 17** and **20-24**) did not show any enhancement of activity. However, compound **18** exhibited significant activity (MIC = 3.12 µg/ml). Such activity might be attributed to the presence of the pharmacophore carbothioamide moiety. It is worth mentioning that *Mtb* is uniquely surrounded by a thick and waxy cell wall, thus, efficient anti-TB drugs should have a reasonable lipophilicity to penetrate the cell wall [55]. Comparison of the logP data, presented in **table 2**, of the most active compounds with those of the reference drugs revealed that compounds **6b,c, 8a-d, 12c** and **14b** were more lipophilic in nature. Also, by correlating their calculated logP and MIC values, it is evident that the most potent compound **8b** was the most lipophilic.

2.2.4. *In vitro* cytotoxicity assay

In order to eliminate the possibility that the anti-TB activity of the tested compounds arises from general toxicity and also to highlight their safety profile on normal cell, the compounds exhibiting significant anti-TB activity **(8a-d, 14b** and **18)** with MIC values ≤ 6.25 µg/ml were further screened for cell viability assay using MTT (3-(4,5-Dimethylthiazol-2-yl)-2,5-diphenyl tetrazolium bromide) assay against peripheral blood mononuclear cells (PBMC). The MTT assay is a quantitative colorimetric assay for assessing cell metabolic activity of enzymes that reduce tetrazolium dye to its insoluble formazan, giving a purple color. Its main application is to assess the viability (cell counting) and the proliferation of cells. It can also be used to determine cytotoxicity of medicinal agents and toxic materials, since those agents would stimulate or inhibit cell viability and growth [56]. The cytotoxicity results of the tested compounds, expressed as inhibitory values (IC_{50} in µg/ml), are presented in **table 3**. The selectivity index (SI) of each compound was also determined as the ratio between *in vitro* cytotoxicity (IC_{50} in

µg/ml) and anti-TB activity (MIC in µg/ml), as shown in **table 3**. SI is used to estimate the therapeutic window of a drug and to identify drug candidates for further studies. According to Orme *et al*. [57], candidates for new anti-TB drugs must have an index equal to or higher than 10, with MIC lower than 6.25 mg/ml and a low cytotoxicity. SI values of compounds equal to or greater than 10 are considered nontoxic. The results revealed that the tested compounds exhibited very low cytotoxicity (IC_{50} value ranging from 589.1 to 1174.6 µg/ml). This also indicated that the active derivatives target *Mtb* to a greater extent compared to normal human cells.

Table 3: Cytotoxicity and selectivity index (SI) for compounds **(8a-d, 14b and 18)** against PBMCs

Compound ID	Cytotoxicity (IC_{50} in µg/ml)	MIC (µg/ml)	Selectivity index (SI)
8a	613.4	3.12	196.6
8b	846.9	0.78	1085.7
8c	642.6	1.56	411.9
8d	1174.6	1.56	752.9
14b	767.8	6.25	122.8
18	589.1	3.12	188.8

2.3. Bioactivity profiling and molecular modeling

2.3.1. Shape-based similarity

In an attempt to elucidate the mechanism of action and identify the putative molecular target behind the antimycobacterial activity of the most active compounds, we followed a sequential scheme combining both ligand-based and structure-based approaches. The first step involved the use of similarity-based method via computation of atom pair Tanimoto coefficient (in ChemMine tools) as a means of comparison and prioritization for structurally-related compounds [58]. This similarity index was measured between the most active compound **8b** and a set of eight pyrazine-based compounds with reported antimycobacterial activity. It is noteworthy to mention that each of these compounds was either tested experimentally or successfully docked into a number of mycobacterial targets as shown in **table 4**. In addition, these targets were selected according to the reported target identification pipeline for *Mtb* [59], in addition to the reported possible targets for PZA (RpsA) [17] and PZA analogs (FAS-1) [60]. These targets represent

various roles in the metabolic pathways of *Mtb*, which could be utilized for the development of new anti-TB agents. For example, FAS-1, InhA, FabH and pantothenate synthase (PS) are involved in fatty acid biosynthesis [61] while RpsA is a vital protein involved in protein translation [17, 62]. Decaprenylphosphoryl-β-D-ribose-2'-epimerase (DprE1) is a potential target essential for cell growth and survival [63] and isocitrate lyase (ICL) is an important enzyme in the glyoxylate cycle during carbohydrate starvation in *Mtb* [64].

Results revealed that compounds **C**, **F** and **G** showed the highest similarity indices in the range of 0.297-0.346. These compounds were reported to exert their antimycobacterial activity via acting on isocitrate lyase (**ICL**), β-ketoacyl-(acyl-carrier-protein) synthase III (**FabH**) and pantothenate synthetase enzymes, respectively. The lowest tanimoto coefficients were recorded for compounds **A** and **B** representing ribosomal protein S1 (**RpsA**) and fatty acid synthase (**FAS I**). Hence, they will be excluded from the next step.

Table 4: Atom pair Tanimoto similarity values with compound **8b** using ChemMine tools.

Code	Structure	AP Tanimoto Similarity with 8b	Potential Anti-TB target	Reference
A	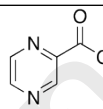	0.067	RpsA	[17]
B	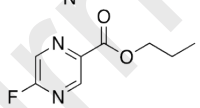	0.061	FAS1	[60]
C	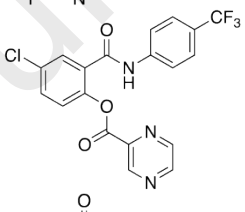	**0.346**	ICL	[65]
D	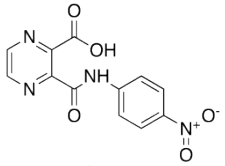	0.236	DprE1	[66]
E	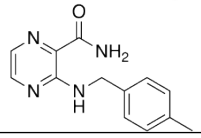	0.204	InhA	[67]

F	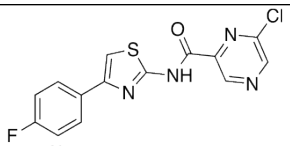	**0.297**	FabH	[68]
G	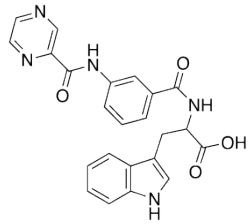	**0.34**	Pantothenate synthetase	[69]
H	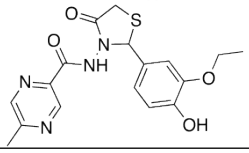	0.204	DprE1	[70]

2.3.2. Pharmacophore mapping

The pharmacophore model was built using molecular operating environment (MOE) software version 2016.0802 [71]. It was derived from the most active six compounds in this study (**8a-d**, **14b** and **18**). The generated model was then tested against compounds **C** – **H**, which passed the similarity searching step.

The pharmacophore Elucidator module of the software MOE was used to obtain the pharmacophore model. It operates first by exhaustively generating pharmacophore queries for a set of flexibly aligned molecules, followed by assigning scores to them based on a joint measure of their cover (how many compounds were used to generate the model out of the initial set), overlap (how well they overlay the ligands) and accuracy (how well they group the dataset into actives and inactives). The selected model (cover = 6, overlap = 4.11, accuracy = 1) is represented in **Figure 3**.

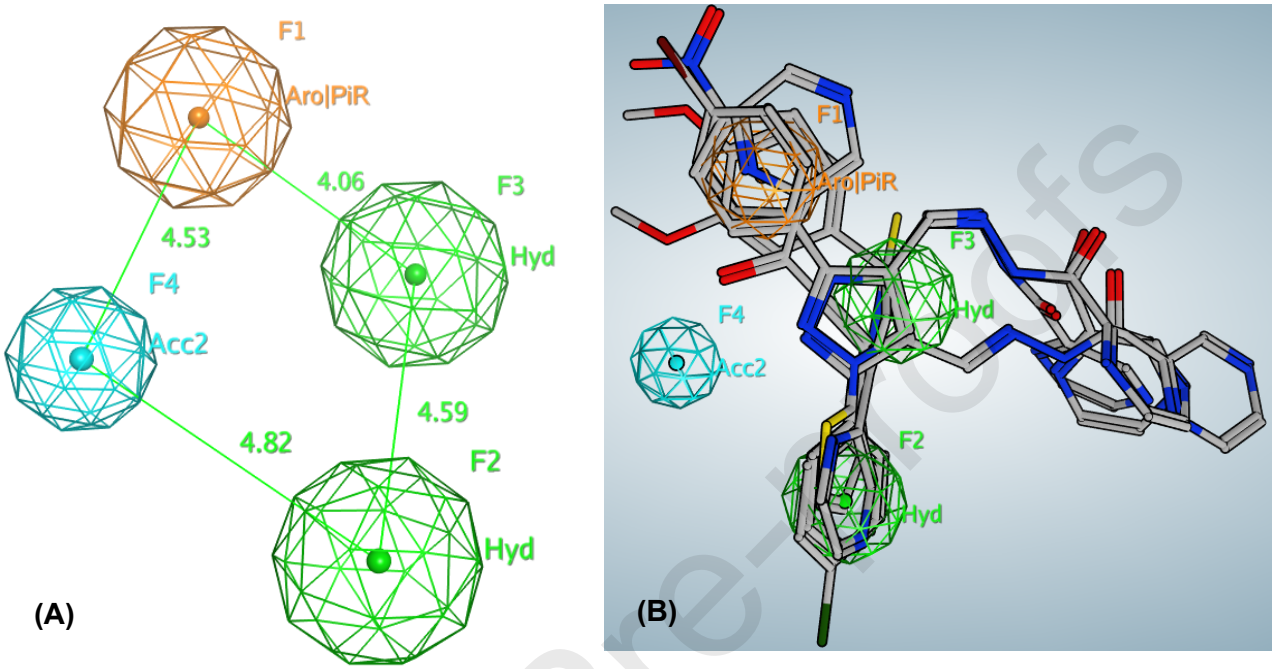

Figure 3. **(A)** Pharmacophore model (F1, orange spherical mesh, aromatic or Pi ring centers), (F2 and F3, green spherical meshes, hydrophobic region) and (F4, cyan spherical mesh, hydrogen bond acceptor projection). **(B)** Overlay of training set compounds (**8a-d**, **14b** and **18**) on the pharmacophore model.

The generated model showed that the following structural features were shared with the six compounds; location of potential aromatic or Pi ring centers (F1, orange spherical mesh), two locations of potential hydrophobic regions (F2 and F3, green spherical meshes) and potential location of hydrogen bond acceptor (F4, cyan spherical mesh).

Using another ligand-based approach to focus the target selection process, mapping of structures **C** – **H**, resulting from the previous step and acting on different five TB targets, on this pharmacophore model was performed. Three of them (**E**, **F** and **G**) showed good fitting with reasonable root-mean-square distance (RMSD) between the model feature and their matching ligand target points in the range of 0.68-0.84 A° (**Table 5**, **Figure SM1A**). This might assume that our target compounds can bind to the proposed receptors with a similar set of interactions. Hence, it can be concluded that pantothenate

synthetase, InhA and FabH are the candidate TB targets for the action of our compounds up to this stage.

Furthermore, flexible alignment tool was utilized to probe similarity between the 3D structures of the most active compounds. The top-ranked alignment with the least strain energy (U= 113.12, F= -127.01, S= -13.89) is depicted in **Figure SM1B**, where a good overlay between the six compounds accounts for their activity. As well, proper alignment (U= 100.64, F= -166.65, S= -66.01) could be observed between the most active compound **8b** and the top-ranked compound **G** from the mapping results (representing pantothenate synthetase) (**Figure SM1C**).

Table 5. Pharmacophore mapping results represented as root-mean-square distance (RMSD) values.

Code	RMSD (A°)
Compound **E**	0.6867
Compound **F**	0.8433
Compound **G**	0.6795

2.3.3. Inverse docking study

Inverse docking is a structure-based target fishing tool which entails the screening of a small-molecule ligand for its binding complementarity against plethora of clinically pertinent macromolecular targets. The output is a set of targets ranked relying on a certain 'score'. The top-scored targets represent potential candidates for binding with the ligand [72].

In this context, in order to find a clue for the mechanism of action of the target compounds, the final step involved an inverse docking study that was conducted on the most active compounds (**8a-d, 14b** and **18**) against five selected *Mtb* targets namely; DprE1 (PDB ID: 4FDO), pantothenate synthetase (PDB ID: 3IVX), FabH (PDB ID: 1U6S), InhA (PDB ID: 4TZK) and isocitrate lyase (PDB ID: 1F8M). The X-ray crystal structures were obtained from the protein data bank (PDB). Docking studies were performed using Molecular operating environment software (MOE 2016.0802).

Pose retrieval was carried out in order to validate the docking procedure. This was done by redocking the co-crystallized ligands and calculating root mean square deviation (RMSD). The predictive capability of a software is confirmed if the deviation is less than 1.5 Å. The redocking of co-crystal ligands to their respective molecular targets reproduced the docking poses with acceptable RMSD values of less than 1.5 Å. Superimposition of the co-crystal ligand of pantothenate synthetase enzyme (PDB ID: 3IVX) and its docked pose is shown as an example in **Figure SM2.**

The docking results were interpreted on the basis of docking score, number of hydrogen bonds formed and hydrophobic interactions of the ligand with the protein and were summarized in **table SM1**. Careful inspection of the docking results revealed that all the target compounds showed good interactions within the active sites of the target proteins (with overall scores spanning from -4.83 to -8.51 Kcal/mol) with the exception of compound **18** docked in the active site of isocitrate lyase enzyme. In order to rationalize the correlation between the *in vitro* anti-TB activity and docking results, a cross observational analysis was performed. The most potent three compounds **(8b, 8c and 8d)** in the *in vitro* anti-TB activity were cross observed with their docking ranks on all the studied target proteins. The results are displayed in **table 6**. Based on the results, the docking pose ranking of the three compounds showed marginal deviation in favor of pantothenate synthetase (PDB ID: 3IVX) and FabH (PDB ID: 1U6S) equally with docking ranks of 1st, 2nd and 3rd when compared with their docking pose rankings of the other studied targets.

Table 6: Cross observational analysis of most active three compounds with their docking ranks against the five studied targets

Studied targets	**Ranking positions based on docking scores**		
(PDB ID)	**8b**	**8c**	**8d**
4FDO	2	4	1
3IVX	**2**	**3**	**1**
1U6S	1	3	2
4TZK	4	3	1
1F8M	4	2	1

Finally, the following conclusion can be derived from this sequential scheme; the pantothenate synthetase inhibitor, compound **G** behaved better than the FabH inhibitor compound **F** both in terms of Tanimoto coefficient and pharmacophore mapping steps. Moreover, it exhibited better docking scores in the inverse docking study (-7.90 to -8.51 for pantothenate synthetase versus -7.16 to -7.75 Kcal/mol for FabH for the most active compounds **8b-d**). Hence, the study suggested that pantothenate synthetase enzyme (PDB ID: 3IVX) might be the plausible target accounting for the *in vitro* anti-TB activity of our compounds.

2.3.4. Docking into pantothenate synthetase active site:

The docking poses were selected within the top-scored conformations with the best binding interactions detected by MOE search algorithm and scoring function. In addition, binding energy scores, formation of hydrogen bonds with the neighboring amino acid residues and the relative positioning of the docked poses in comparison with the co-crystallized ligand were the factors determining the binding affinities to the binding pocket of the enzyme.

Generally speaking, the target compounds (**8a-d, 14b** and **18**) interacted via hydrogen bonding and hydrophobic contacts with the key amino acid residues that were also involved in the binding of the native ligand such as His47, Gly158Lys160, Ser197 (for **8b**), His44, His47, Gly158 (for **14b**) and His44, His47, Gly158, Ser197 (for **18**). In addition, they established some additional interactions that account for further stabilization of the formed complexes as shown in **table SM2**, **Figures 4-6** for compounds **8b**, **14b** and **18**, and **Figures SM3-SM5** for compounds **8a,c,d**. Moreover, it was evident from the overlay of the compounds over the co-crystallized ligand FG6 that they occupied the same spatial area of the binding pocket of the enzyme.

In details, the most energetically profitable pose of compound **8b** extended smoothly in the active site through the formation of two hydrogen bonds between two nitrogens of the acid hydrazide part and Ser197. The carbonyl oxygen also engaged in hydrogen bond with Lys160. Binding was also strengthened by the formation of two arene-hydrogen interactions between the phenyl ring and Gly46 and Gly158. Two arene-hydrogen

contacts were also observed between p-bromophenyl and pyrazine rings and His47 and Arg198 residues, respectively (**Figure 4**). As for the chalcone **14b**, one of the pyrazine nitrogens was hydrogen bonded to His47 while the sulfur atom formed two hydrogen bonds with Val187 and Met195. As well, one of the hydrogens of ⟨,®-unsaturated carbonyl moiety attached via hydrogen bond to Met195. Moreover, the thiophene ring interacted with the surrounding hydrophobic residues (His44, Gly46, Gly158 and Thr186) through arene-hydrogen interactions (**Figure 5**). Regarding docking of the pyrazoline thioamide derivative **18**, it was well-fitted in the active site cavity and showed almost the same binding pattern of the native ligand. The complex formed was stabilized by a number of interactions with some important residues in close proximity. For example, pyrazine ring was held in the active site via two arene-hydrogen interactions with His44 and Gly158. The amino group was hydrogen bonded to His47 and Tyr82. Furthermore, sulfur atom was hydrogen-bonded to His44 and Ser197. Hydrogen bonding was also observed between one of the aromatic hydrogens of the dimethoxy phenyl ring and Pro38 (**Figure 6**).

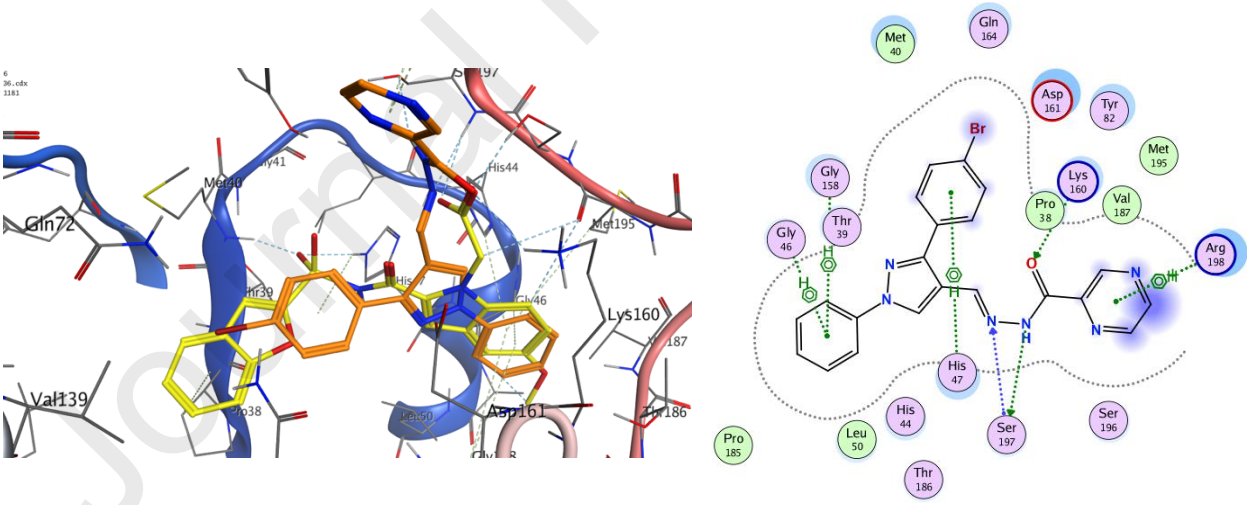

Figure 4. Docking and binding pattern of compound **8b** (in orange) into pantothenate synthetase active site (PDB 3IVX) and its overlay over FG6 (in yellow) in 3D (left panel). Ligand interactions in 2D (right panel).

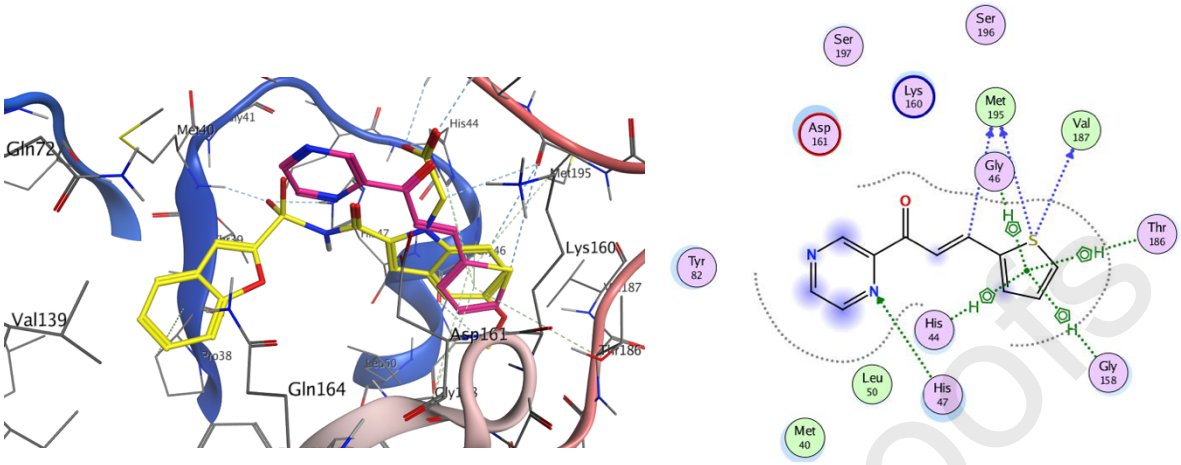

Figure 5. Docking and binding pattern of compound **14b** (in pink) into pantothenate synthetase active site (PDB 3IVX) and its overlay over FG6 (in yellow) in 3D (left panel). Ligand interactions in 2D (right panel).

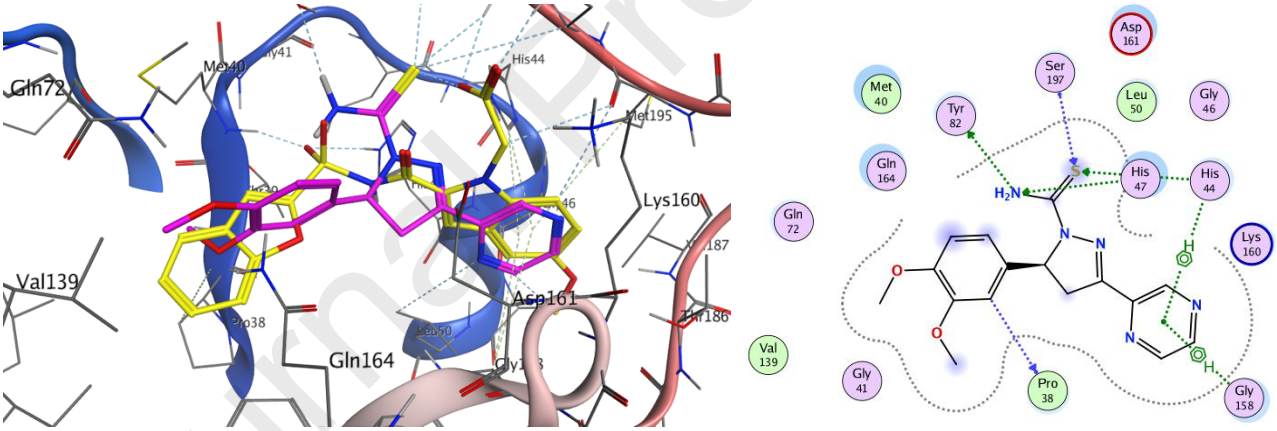

Figure 6. Docking and binding pattern of compound **18** (in pink) into pantothenate synthetase active site (PDB 3IVX) and its overlay over FG6 (in yellow) in 3D (left panel). Ligand interactions in 2D (right panel).

2.4. *In silico* prediction of drug-likeness, physicochemical properties and pharmacokinetic profile

ADME, as well as toxicological profile, are important for the ultimate success or failure of a possible drug candidate. Adverse effects in animal models or even clinical trials can be reduced by filtering drug candidates by their ADME properties in early stages. Thus, *in*

silico ADMET prediction will permit the parallel optimization of compound efficacy and drug suitability, which is expected to not only improve the overall quality of drug candidates and therefore the probability of their success, but also to lower the overall expenses due to a reduced downstream attrition rate [73].

In the present work, compounds (**8a**-**d** and **18**) that displayed significant anti-TB activity with MIC values ≤ 3.12 µg/ml, were subjected to physicochemical properties prediction using Data Warrior software from Osiris property explorer [74], in order to filter and analyze the overall potential of these compounds to qualify for a drug, also comparing them to some current anti-TB drugs. The results are recorded in **table 7**.

Table 7: *In silico* physicochemical properties of the most active compounds

Comp. ID	M.Wt[a]	CLog P[b]	S[c]	HBA[d]	HBD[e]	Lipinski's violation	TPSA[f]	%ABS[g]	NROTB[h]
8a	368.39	2.17	8.38	7	1	0	85.06	79.65	5
8b	447.29	2.89	0.72	7	1	0	85.06	79.65	5
8c	382.42	2.51	3.05	7	1	0	85.06	79.65	5
8d	447.84	1.85	0.36	10	1	0	130.88	63.84	6
18	343.41	0.91	94.35	7	1	0	117.95	68.30	4
INH	137.14	-1.02	8568	4	2	0	68.01	85.53	1
PZA	123.11	-1.20	35913	4	1	0	68.87	85.23	1

[a] **M.Wt:** Molecular weight.
[b] **LogP:** Logarithm of compound partition coefficient between n-octanol and water.
[c] **S:** Compound's solubility in mg/L.
[d] **HBA:** Number of hydrogen bond acceptors.
[e] **HBD:** Number of hydrogen bond donors.
[f] **TPSA:** Topological polar surface area.
[g] **%ABS:** Percentage of absorption after oral administration.
[h] **NROTB:** Number of rotatable bonds.

The results revealed that the tested compounds were shown to possess one H-bond donor and acceptable range of H-bond acceptors (7-10). The compounds also displayed logP values in the range from 0.91 to 2.89. and molecular weights of less than 500. Hence, the physicochemical parameters of the tested molecules were encouraging with zero Lipinski violation.

Number of rotatable bonds is important for conformational changes and ultimately for the binding to receptors or channels. Tested compounds possessed (4–6) rotatable bonds and therefore exhibiting moderate conformational flexibility. The results showed that all tested compounds demonstrated TPSA values within allowable range (85.06–130.88) and generally displayed % ABS range of 63.84–79.65%, which indicated their good bioavailability by oral administration. Furthermore, compounds **(8a, 8c and 18)** were found to fulfill the requirements of solubility of more than 0.0001 mg/L [75, 76] and could be considered as drug candidates for oral absorption.

Although Lipinski's "Rule of 5" describes the molecular properties important for a drug's pharmacokinetics in the human body, it does not predict the toxicity profile of the compounds. Therefore, mutagenicity, tumorigenicity, irritation effect, and risk of reproductive effect were also predicted for toxicity study using Osiris DataWarrior. The toxicity results as well as computed drug-likeness scores are recorded in **table 8**.

Table 8: Toxicity prediction and drug-likeness scores of the most active compounds

Comp. ID	Drug-likeness score	Toxicity			
		Mutagenic	Tumorigenic	Reproductive effect	Irritant
8a	5.91	None	None	None	None
8b	4.12	None	None	None	None
8c	5.82	None	None	None	None
8d	0.78	None	None	None	None
18	2.59	None	None	High	None
INH	-5.78	High	High	High	High
PZA	-0.67	High	High	High	High

The results indicated that all tested compounds lacked mutagenic, tumorigenic, irritant, reproductive effect properties, except for compound **18** which demonstrated high risk of reproductive effect. In addition, the tested compounds showed good safety profile compared to the tested reference drugs. Regarding drug-likeness scores, the investigated compounds should be considered as drug-like as they have positive values in the range 0.78-5.91.

Furthermore, Pre-ADMET calculator [77] was used to calculate ADME properties of the active compounds. The value of each of the following parameters was calculated and

compared with the optimal values of the following properties: Caco2 cell permeability coefficient (permeability through cells derived from human colon adenocarcinoma), Madin-Darby canine kidney (MDCK) cell permeability coefficient, blood–brain barrier (BBB) coefficient and plasma protein binding (PPB). The results are given in **table 9**.

Table 9: *In silico* ADME profiling of the most active compounds

Comp. ID	Caco2[a]	MDCK[b]	HIA[c]	BBB[d]	PPB[e]
8a	20.59	137.10	96.50	0.08	91.24
8b	23.01	0.03	96.71	0.06	100.00
8c	23.51	17.18	96.46	0.07	89.90
8d	16.20	0.07	97.73	0.11	97.71
18	21.83	121.28	98.03	0.07	78.05
INH	19.49	0.81	87.10	0.26	1.60
PZA	16.43	119.55	87.45	0.15	0.711

[a] **Caco2:** Permeability through cells derived from human colon adenocarcinoma; Caco2 values < 4 nm/sec (low permeability), values from 4 to 70 nm/sec (medium permeability) and values > 70 nm/sec (high permeability).
[b] **MDCK:** Permeability through Madin–Darby canine kidney cells; MDCK values < 25 nm/sec (low permeability), values from 25 to 500 nm/sec (medium permeability) and values > 500 nm/sec (high permeability).
[c] **HIA:** Percentage human intestinal absorption; HIA values from 0 to 20% (poorly absorbed), values from 20 to 70% (moderately absorbed) and values from 70 to 100% (well absorbed).
[d] **BBB:** Blood–brain barrier penetration; BBB values < 0.1 (low CNS penetration), values from 0.1 to 2 (medium CNS absorption) and values > 2 (high CNS absorption)
[e] **PPB:** Plasma protein binding; PPB values < 90 % (poorly bound) and > 90% (strongly bound).

The *in silico* ADME results indicated that all tested compounds showed medium cell permeability in the Caco2 cell model with values from 16.20 to 23.51 nm/sec. Additionally, compounds **8a** and **18** displayed medium cell permeability in the MDCK cell model, while compounds **8b, 8c** and **8d** showed low permeability in this model.

Furthermore, the predicted oral bioavailability was excellent as all tested molecules exerted high HIA values from 96.46 to 98.23 % indicating very well absorbed compounds. Additionally, all tested compounds displayed low BBB penetration capability (0.06-0.08) except for compound **8d** (0.11). In addition, compounds **8c** and **18** were found to be

weakly-bound to plasma proteins, whereas the rest were more than 90% bound. Moreover, CYP2D6 enzyme is responsible for metabolism as well as excretion of approximately 25% of clinically used drugs. The tested compounds showed no inhibition of this enzyme, thus they may be metabolized and excreted successfully.

3. Conclusion

In this study, various pyrazine derivatives have been developed as new anti-TB chemotypes. The synthesized compounds were subjected to *in silico* activity prediction using PASS analysis. Thirty-one compounds showed anti-TB activity with reasonable Pa values and were further screened *in vitro* against *Mtb* $H_{37}RV$ strain using MABA assay. Six compounds (**8a**, **8b**, **8c**, **8d**, **14b** and **18**) displayed significant activity against *Mtb* with MIC values ≤ 6.25 µg/ml. Compound **8b** exhibited anti-TB activity higher than the two references PZA and EMB (MIC = 0.78 µg/ml). Compounds **8c** and **8d** showed higher potency than PZA and equal to that of EMB (MIC = 1.56 µg/ml). In addition, compounds **8a** and **18** were more active than PZA (MIC = 3.12 µg/ml), while compound **14b** was equipotent to PZA. Structure-activity correlation for the anti-mycobacterial activity of these active derivatives has been analyzed and revealed that the presence of a linker between the pyrazine ring and other heterocyclic moieties was necessary for biological activity, while direct attachment led to loss of activity. Moreover, the *in vitro* cytotoxicity of the most active compounds **8a-d**, **14b** and **18** against PBMC normal cell line was evaluated using MTT assay and no cytotoxicity was detected for the tested concentrations and the estimated IC_{50} values were in the range of 589.1-1174.6 µg/ml, indicating satisfactory safety profile and selectivity (SI ≥ 200). In an attempt to get some clues on the potential target behind the antimycobacterial activity of the most active compounds, a target fishing approach was adopted. It started with calculating similarity index between our most active compound **8b** and some reported pyrazine derivatives with verified molecular targets. Secondly, a pharmacophore mapping study was conducted using a pharmacophore model from our most active compounds and the reported pyrazine derivatives that passed the first step. Finally, an inverse docking study was employed. All the three steps combined suggested pantothenate synthetase as a potential target. Docking of the most active compounds in the active site of the enzyme demonstrated favorable binding modes and interaction patterns. *In silico* prediction of physicochemical,

ADMET and drug-like properties were assessed and revealed that most of the tested compounds were found to be within those considered adequate for a drug candidate. Hence, these compounds could represent a promising template for the development of antimycobacterial agents with improved activity.

4. Experimental

4.1. Chemistry

Melting points were recorded on electrotherm capillary tube Stuart melting point apparatus SMP10 and are all uncorrected. Follow up of the reactions' rates were performed by thin-layer chromatography (TLC) on silica gel precoated aluminum sheets (Type 60 GF254; Merck; Germany) and the spots were visualized by exposure to iodine vapors or UV-lamp at λ 254nm for few seconds. Infrared spectra (IR) were recorded using KBr discs on a PerkinElmer IR spectrophotometer, Faculty of Pharmacy, Alexandria University and on Schimadzu FT-IR Affinity-1 spectrometer at the microanalytical unit, Faculty of Pharmacy, Cairo University. Nuclear magnetic resonance (^{1}H NMR and ^{13}C NMR) spectra were recorded on a Jeol spectrophotometer (500 MHz), Faculty of Science, Alexandria University and on a Bruker spectrophotometer (400 MHz), Faculty of Pharmacy, Cairo University using deuterated dimethylsulfoxide (DMSO-d_6) and deuterated chloroform ($CDCl_3$) as solvents, followed by recording the spectra again after addition of D_2O for detection of D_2O exchangeable peaks. The data were recorded as chemical shifts expressed in δ (ppm) relative to tetramethylsilane (TMS) as internal standard. Signal splitting are expressed by the following abbreviations: s = singlet, d = doublet, t = triplet, q = quartet and m = multiplet. Microanalytical data (C, H, N and S) were performed on FLASH 2000 CHNS/O analyzer, Thermo Scientific at the regional center for mycology and biotechnology (RCMB), Al-Azhar University. Compounds **2**, **3, 5** and **7a-d** were prepared according to reported procedures [28, 43, 78-81].

4.1.1. General procedure for synthesis of compounds 6a-c and 8a-d:

To a stirred solution of the acid hydrazide **5** (2 mmol, 0.27 g) in absolute ethanol (10 ml), the appropriate heteroaromatic ketone or substituted pyrazolaldehyde (2 mmol) was added in the presence of catalytic amount of glacial acetic acid (5 drops), the mixture was

refluxed for 12-16 h. The product obtained was filtered, washed with diethyl ether, dried and recrystallized from ethanol.

4.1.1.1. (*E*)-N'-[1-(2-Pyrazinyl)ethylidene]pyrazine-2-carbohydrazide **(6a)**.

White powder, yield 87%. m.p.278~280 °C. IR (KBr, cm^{-1}): 3379.29 (enolic OH), 3321.42 (NH), 1701.22 (C=O), 1508.33 (C=N). ^{1}H NMR (400 MHz, DMSO-d_6): δ 2.57 (s, 3H, CH_3), 8.84 (d, J = 4 Hz, 1H, pyrazine-$C_{6'}$-H), 8.88 (d, *J* = 4 Hz, 1H, pyrazine-$C_{5'}$-H), 8.95 (d, *J* = 2.3 Hz, 1H, pyrazine-C_6-H), 8.97-8.98 (m, 1H, pyrazine-C_5-H), 9.15 (s, 1H, pyrazine-$C_{3'}$-H), 9.31 (s, 1H, pyrazine-C_3-H), 11.24 (s, 1/3 H, NH, D_2O exchangeable), 15.39 (s, 2/3 H, enolic OH, D_2O exchangeable). ^{13}C NMR (100 MHz, DMSO-*d_6*): δ 22.4 (CH_3), 142.8 (pyrazine-C3'), 144.2 (pyrazine-C5'), 144.4 (pyrazine-C3, C5), 145.8 (C=N), 146.1 (pyrazine-C6, C6'), 148.6 (pyrazine-C2,2'), 160.1 (C=O). EI-MS: m/z (242.12) ($M^{+\bullet}$). Anal. Calcd (%) for $C_{11}H_{10}N_6O$ (242.24): C, 54.54; H, 4.16; N, 34.69. Found: C, 54.31; H, 4.29; N, 34.84.

4.1.1.2. (*E*)-N'-[1-(3-Pyridinyl)ethylidene]pyrazine-2-carbohydrazide **(6b).**

White powder, yield 81%. m.p.218~220 °C. IR (KBr, cm^{-1}): 3336.86 (enolic OH), 3321.42 (NH), 1693.50 (C=O), 1516.05 (C=N). ^{1}H NMR (400 MHz, DMSO-d_6): δ 2.45 (s, 3H, CH_3), 7.51 (t, *J* = 4 Hz, 1H, pyridine-C_5-H), 8.25 (d, *J* = 8 Hz, 1H, pyridine-C_4-H), 8.65 (d, *J* = 4 Hz, 1H, pyridine-C_6-H), 8.83 (brs, 1H, pyrazine-C_6-H), 8.96 (brs,1H,pyrazine-C_5-H), 9.05 (brs, 1H, pyridine-C_2-H), 9.29 (s, 1H, pyrazine-C_3-H), 11.15 (s, 1H, NH, D_2O exchangeable). ^{13}C NMR (100 MHz, DMSO-*d6*): δ 14.3 (CH_3), 124.0 (pyridine-C_5), 133.7 (pyridine-C_3), 134.3 (pyridine-C_4), 143.9 (pyrazine-C_5), 144.3 (pyrazine-C_3), 145.0 (pyrazine-C_2), 148.1 (pyrazine-C_6), 148.4 (pyridine-C_2), 150.9 (pyridine-C_6), 154.7 (C=N), 159.7 (C=O). Anal. Calcd (%) for $C_{12}H_{11}N_5O$ (241.25): C, 59.74; H, 4.60; N, 29.03. Found: C, 59.98; H, 4.61; N, 29.41.

4.1.1.3. (*E*)-N'-[1-(4-Pyridinyl)ethylidene]pyrazine-2-carbohydrazide **(6c).**

White powder, yield 64%. m.p.222~224 °C. IR (KBr, cm^{-1}): 3336.85 (enolic OH), 3305.99 (NH), 1701.22 (C=O), 1577.77 (C=N). ^{1}H NMR (400 MHz, DMSO-d_6): δ 2.42 (s, 3H, CH_3), 7.81 (d, *J* = 4 Hz, 2H, pyridine-$C_{3,5}$-H), 8.68 (d, *J* = 8 Hz, 2H, pyridine-$C_{2,6}$-H), 8.83 (brs,1H, pyrazine-C_6-H), 8.96 (d, *J* = 2.24 Hz, 1H, pyrazine-C_5-H), 9.29 (s, 1H, pyrazine-C_3-H), 11.17 (s, 1H, NH, D_2O exchangeable). EI-MS: m/z (241.97) ($M^{+\bullet}$). Anal. Calcd (%) for $C_{12}H_{11}N_5O$ (241.25): C, 59.74; H, 4.60; N, 29.03. Found: C, 59.87; H, 4.53; N, 29.35.

4.1.1.4. (*E*)-N'-[(1,3-diphenyl-1*H*-pyrazol-4-yl)methylene]pyrazine-2-carbohydrazide **(8a).**

White powder, yield 67%. m.p.243~245 °C. IR (KBr, cm^{-1}): 3309.85 (NH), 1678.07 (C=O), 1597.06 (C=N). ^{1}H NMR (400 MHz, DMSO-d_6): δ 7.39 (t, *J* = 8 Hz, 1H, phenyl-$C_{4'}$-H), 7.48-7.57 (m, 5H, phenyl-$C_{3,4,5}$-H and phenyl-$C_{3',5'}$-H), 7.78 (d, *J* = 8 Hz, 2H, phenyl-$C_{2,6}$-H), 8.05 (d, *J* = 8 Hz, 2H, phenyl-$C_{2',6'}$-H), 8.77-8.78 (m, 1H, pyrazine-C_6-H), 8.84 (s, 1H, CH=N-), 8.92 (d, *J* = 4 Hz, 1H, pyrazine-C_5-H), 9.03 (s, 1H, pyrazole-C_5-H), 9.28 (s, 1H, pyrazine-C_3-H), 12.33 (s, 1H, NH, D_2O exchangeable). ^{13}C NMR (100 MHz, DMSO-*d6*): δ 117.2 (pyrazole-C_4), 119.3 (phenyl-$C_{2,6}$), 127.5 (phenyl-C_4), 127.7 (phenyl-$C_{2',6'}$), 128.9 (phenyl-$C_{4'}$), 129.0 (phenyl-$C_{3',5'}$), 129.2 (phenyl-$C_{3,5}$), 130.0 (pyrazole-C_5), 132.3 (phenyl-$C_{1'}$), 139.5 (phenyl-C_1), 143.6 (CH=N), 144.5 (pyrazine-$C_{3,5}$), 145.2 (pyrazine-C_2), 148.2 (pyrazine-C_6), 152.4 (pyrazole-C_3), 159.5 (C=O). Anal. Calcd (%) for $C_{21}H_{16}N_6O$ (368.39): C, 68.47; H, 4.38; N, 22.81. Found: C, 68.80; H, 4.51; N, 23.08.

4.1.1.5. (*E*)-N'-[(3-(4-bromophenyl)-1-phenyl-1*H*-pyrazol-4-yl)methylene]pyrazine-2-carbohydrazide **(8b).**

White powder, yield 80%. m.p.230~232 °C. IR (KBr, cm^{-1}): 3267.41 (NH), 1678.07 (C=O), 1597.06 (C=N). ^{1}H NMR (400 MHz, DMSO-d_6): δ 7.39 (t, *J* = 8 Hz, 1H, phenyl-C_4-H), 7.53-7.78 (m, 6H, phenyl-$C_{2,3,5,6}$-H and 4-bromophenyl-$C_{3,5}$-H), 8.04 (d, *J* = 8 Hz, 2H, 4-bromophenyl-$C_{2,6}$-H), 8.78 (brs, 1H, pyrazine-C_6-H), 8.80 (s, 1H, CH=N-), 8.93 (d, *J* = 2.12 Hz, 1H, pyrazine-C_5-H), 9.04 (s, 1H, pyrazole-C_5-H), 9.28 (s, 1H, pyrazine-C_3-H), 12.30 (s, 1H, NH, D_2O exchangeable). ^{13}C NMR (100 MHz, DMSO-*d6*): δ 117.3 (pyrazole-

C_4), 119.3 (phenyl-$C_{2,6}$), 122.5 (4-bromophenyl-C_4), 127.5 (phenyl-C_4), 128.2 (4-bromophenyl-$C_{2,6}$), 130.0 (phenyl-$C_{3,5}$), 130.9 (pyrazole-C_5), 131.6 (4-bromophenyl-C_1), 132.0 (4-bromophenyl-$C_{3,5}$), 139.4 (phenyl-C_1), 143.3 (CH=N), 143.7 (pyrazine-C_5), 144.5 (pyrazine-C_3), 145.1 (pyrazine-C_2), 148.2 (pyrazine-C_6), 151.1 (pyrazole-C_3), 159.5 (C=O). EI-MS: m/z (447.94) ($M^{+\bullet}$). Anal. Calcd (%) for $C_{21}H_{15}BrN_6O$ (447.29): C, 56.39; H, 3.38; N, 18.79. Found: C, 56.18; H, 3.29; N, 19.01.

4.1.1.6. (*E*)-N'-[(1-phenyl-3-(p-tolyl)-1*H*-pyrazol-4-yl)methylene]pyrazine-2-carbohydrazide **(8c).**

White powder, yield 63%. m.p.218~222 °C. IR (KBr, cm^{-1}): 3263.56 (NH), 1678.07 (C=O), 1597.06 (C=N). ^{1}H NMR (400 MHz, DMSO-d_6): δ 2.39 (s, 3H, CH_3), 7.34-7.56 (m, 5H, 4-tolyl-$C_{3,5}$-H and phenyl-$C_{3,4,5}$-H), 7.67 (d, *J* = 8 Hz, 2H, phenyl-$C_{2,6}$-H), 8.04 (d, *J* = 8 Hz, 2H, 4-tolyl-$C_{2,6}$-H), 8.78 (brs, 1H, pyrazine-C_6-H), 8.82 (s, 1H, CH=N-), 8.92 (d, *J* = 2.28 Hz, 1H, pyrazine-C_5-H), 9.00 (s, 1H, pyrazole-C_5-H), 9.28 (s, 1H, pyrazine-C_3-H), 12.30 (s, 1H, NH, D_2O exchangeable). ^{13}C NMR (100 MHz, DMSO-*d6*): δ 21.3 (CH_3), 117.1 (pyrazole-C_4), 119.3 (phenyl-$C_{2,6}$), 127.4 (phenyl-C_4), 127.6 (4-tolyl-C_1), 128.7 (4-tolyl-$C_{2,6}$), 129.5 (pyrazole-C_5), 129.7 (phenyl-$C_{3,5}$), 130.0 (4-tolyl-$C_{3,5}$), 138.5 (4-tolyl-C_4), 139.5 (phenyl-C_1), 143.7 (CH=N), 143.8 (pyrazine-C_5), 144.5 (pyrazine-C_3), 145.2 (pyrazine-C_2), 148.2 (pyrazine-C_6), 152.4 (pyrazole-C_3), 159.5 (C=O). Anal. Calcd (%) for $C_{22}H_{18}N_6O$ (382.42): C, 69.10; H, 4.74; N, 21.98. Found: C, 68.89; H, 4.86; N, 22.23.

4.1.1.7. (*E*)-N'-[(3-(4-chlorophenyl)-1-(4-nitrophenyl)-1*H*-pyrazol-4-yl)methylene] pyrazine-2-carbohydrazide **(8d).**

Orange powder, yield 86%. m.p.>300 °C. IR (KBr, cm^{-1}): 3298.28 (NH), 1693.50 (C=O), 1593.20 (C=N). ^{1}H NMR (400 MHz, DMSO-d_6): δ 7.59 (d, *J* = 4 Hz, 2H, 4-chlorophenyl-$C_{3,5}$-H), 7.82 (d, *J* = 8 Hz, 2H, 4-chlorophenyl-$C_{2,6}$-H), 8.30-8.37 (m, 4H, 4-nitrophenyl-$C_{2,3,5,6}$-H), 8.78 (brs, 2H, pyrazine-$C_{5,6}$-H), 8.93 (s, 1H, CH=N-), 9.22 (s, 1H, pyrazole-C_5-H), 9.28 (s, 1H, pyrazine-C_3-H), 12.33 (s, 1H, NH, D_2O exchangeable). Anal. Calcd (%) for $C_{21}H_{14}ClN_7O_3$ (447.83): C, 56.32; H, 3.15; N, 21.89. Found: C, 56.54; H, 3.27; N, 21.76.

4.1.2. 2-Cyano-N'-[1-(pyrazin-2-yl)ethylidene]acetohydrazide **(9).**

A mixture of cyanoacetic acid hydrazide (1 mmol, 0.1 g) and 2-acetylpyrazine **(2)** (1 mmol, 0.12 g) in absolute ethanol (4 ml) was refluxed for 1 h. On cooling to room temperature, the crystalline product separated was filtered, washed with ethanol, dried, and recrystallized from dioxane.

White crystals, yield 75%. m.p.228~230 °C. IR (KBr, cm^{-1}): 3356.69 (NH), 2261.19 (C≡N), 1685.56 (C=O), 1619.59 (C=N). ^{1}H NMR (500 MHz, DMSO-d_6): δ 2.28 (s, 3H, CH_3), 4.33 (s, 2H, CH_2CN), 8.56-8.60 (m, 2H, pyrazine-$C_{5,6}$-H), 9.30 (s, 1H, pyrazine-C_3-H), 11.34 (s, 1H, NH, D_2O exchangeable). ^{13}C NMR (100 MHz, DMSO-*d6*): δ 12.3 (CH_3), 25.4 (CH_2 – CN), 116.6 (CN), 143.0 (pyrazine – C_3), 143.6 (pyrazine – C_6), 144.6 (pyrazine – C_5), 148.3 (CH_3-C=N), 150.5 (pyrazine – C_2), 166.7 (C=O). EI-MS: m/z (203.10) ($M^{+\bullet}$). Anal. Calcd (%) for $C_9H_9N_5O$ (203.20): C, 53.20; H, 4.46; N, 34.47. Found: C, 53.48; H, 4.53; N, 34.72.

4.1.3. 2-Imino-N'-[1-(pyrazin-2-yl)ethylidene]-2*H*-chromene-3-carbohydrazide **(10).**

To a stirred solution of compound **9** (1 mmol, 0.2 g) in absolute ethanol (5 ml) was added an equivalent amount of salicylaldehyde (1 mmol, 0.12 g) and few drops of piperidine (2 drops). The reaction mixture was stirred at room temperature for 2 h. The product separated was filtered, washed with ethanol, dried and crystallized from dioxane.

White crystals, yield 76%. m.p.233~235 °C. IR (KBr, cm^{-1}): 3363.11, 3316.21 (NH), 1679.76 (C=O), 1601.15 (C=N). ^{1}H NMR (500 MHz, DMSO-d_6): δ 2.35 (s, 3H, CH_3), 7.22-7.28 (m, 2H, chromene-$C_{6,8}$-H), 7.56 (t, *J* = 5 Hz, 1H, chromene-C_7-H), 7.82 (d, *J* = 5 Hz, 1H, chromene-C_5-H), 8.61 (d, *J* = 10 Hz, 2H, pyrazine-$C_{5,6}$-H), 8.64 (s, 1H, chromene-C_4-H), 9.23 (s, 1H, pyrazine-C_3-H), 9.33 (s, 1H, =NH, D_2O exchangeable), 13.82 (s, 1H, NHCO, D_2O exchangeable). Anal. Calcd (%) for $C_{16}H_{13}N_5O_2$ (307.31): C, 62.53; H, 4.26; N, 22.79. Found: C, 62.80; H, 4.34; N,23.15.

4.1.4. 2-Oxo-N'-[1-(pyrazin-2-yl)ethylidene]-2*H*-chromene-3-carbohydrazide **(11).**

A solution of compound **10** (1 mmol, 0.3 g) in a mixture of ethanol, water, and 32%HCl (30:1:1; v/v/v) was refluxed with stirring for 1 h. The crystalline product separated was filtered, washed with ethanol, dried and recrystallized from dioxane.

Yellow crystals, yield 75%. m.p.297~299 °C. IR (KBr, cm^{-1}): 3362.83 (NH), 1700.01 (lactone C=O), 1608.45 (amide C=O), 1562.41 (C=N). ^{1}H NMR (400 MHz, DMSO-d_6): δ 2.45 (s, 3H, CH_3), 7.50 (t, *J* = 8 Hz, 1H, chromene-C_6-H), 7.59 (d, *J* = 8 Hz, 1H, chromene-C_8-H), 7.82 (t, *J* = 8 Hz, 1H, chromene-C_7-H), 8.10 (d, *J* = 8 Hz, 1H, chromene-C_5-H), 8.70 (d, *J* = 8 Hz, 2H, pyrazine-$C_{5,6}$-H), 9.07 (s, 1H, chromene-C_4-H), 9.28 (s, 1H, pyrazine-C_3-H), 11.84 (s, 1H, NH, D_2O exchangeable). EI-MS: m/z (308.18) ($M^{+\bullet}$). Anal. Calcd (%) for $C_{16}H_{12}N_4O_3$ (308.29): C, 62.33; H, 3.92; N, 18.17. Found: C, 62.24; H, 3.99; N, 18.48.

4.1.5. General procedure for synthesis of compounds 12a-e:

To a stirred solution of **9** (1mmol, 0.2 g), finely divided sulfur (1 mmol, 0.032g) and triethylamine (0.2 ml) in a mixture of dimethylformamide (1 ml) and ethanol (4 ml), the appropriate isothiocyanate (1 mmol) was added dropwise. The reaction mixture was heated under reflux for 1 h during which crystalline product was seperated. The reaction mixture was allowed to cool and the formed product was filtered, washed with ethanol, dried and recrystallized from dioxane.

4.1.5.1. 3-Allyl-4-amino-N'-(1-(pyrazin-2-yl)ethylidene)-2-thioxo-2,3-dihydrothiazole-5-carbohydrazide **(12a).**

Yellowish brown crystals, yield 50%. m.p.235~237 °C. IR (KBr, cm^{-1}): 3410.15 (enolic OH), 3278.99, 3159.40, 3101.54 (NH), 1635.64 (C=O), 1570.06 (C=N),

1234.44 (C=S). ^{1}H NMR (400 MHz, DMSO-d_6): δ 2.37 (s, 3H, CH_3), 4.92 (d, *J* = 5 Hz, 2H, $C\underline{H}_2$ – CH=CH_2), 5.04, 5.19 (2d, *J* = 17 Hz, 10 Hz, 2H, CH_2 – CH=$C\underline{H}_2$), 5.86-5.91 (m, 1H, CH_2 – $C\underline{H}$=CH_2), 8.02 (s,2H, NH_2, D_2O exchangeable), 8.66 (d, *J* = 4 Hz 1H, pyrazine-

C_6-H), 8.69 (m,1H, pyrazine-C_5-H), 9.30 (s,1H,pyrazine-C_3-H), 10.84 (s, 1H, NHCO, D_2O exchangeable). Anal. Calcd (%) for $C_{13}H_{14}N_6OS_2$ (334.42): C, 46.69; H, 4.22; N, 25.13; S, 19.18. Found: C, 46.43; H, 4.37; N, 25.40; S, 19.25.

4.1.5.2. 4-Amino-3-phenyl-N'-(1-(pyrazin-2-yl)ethylidene)-2-thioxo-2,3-dihydrothiazole-5-carbohydrazide **(12b).**

Yellow crystals, yield 43%. m.p.254~256 °C. IR (KBr, cm^{-1}): 3375.43 (enolic OH), 3263.56, 3224.98, 3190.26 (NH), 1631.78 (C=O), 1562.34 (C=N),

1242.16 (C=S). ^1H NMR (400 MHz, DMSO-d_6): δ 2.39 (s, 3H, CH_3), 7.38 (d, *J* = 4 Hz, 2H, phenyl-$C_{2,6}$-H), 7.41 (s, 2H, NH_2, D_2O exchangeable), 7.58–7.66 (m, 3H, phenyl-$C_{3,4,5}$-H), 8.67 (d, *J* = 2.5 Hz, 1H, pyrazine-C_6-H), 8.70-8.71 (m, 1H, pyrazine-C_5-H), 9.33 (s, 1H, pyrazine-C_3-H), 10.91 (s, 2/3 H, NHCO, D_2O exchangeable), 13.11 (s, 1/3 H, enolic OH, D_2O exchangeable). Anal. Calcd (%) for $C_{16}H_{14}N_6OS_2$ (370.45): C, 51.87; H, 3.81; N, 22.69; S, 17.31. Found: C, 51.89; H, 3.97; N, 23.05; S, 17.43.

4.1.5.3. 4-Amino-3-(4-chlorophenyl)-N'-(1-(pyrazin-2-yl)ethylidene)-2-thioxo-2,3-dihydrothiazole-5-carbohydrazide **(12c).**

Yellow crystals, yield 65%. m.p.258~260 °C. IR (KBr, cm^{-1}): 3448.00 (enolic OH), 3352.87 ,3280.46, 3162.01 (NH), 1620.56 (C=O), 1543.60 (C=N), 1237.82 (C=S). ^1H NMR (400 MHz, DMSO-d_6): δ 2.38 (s, 3H, CH_3), 7.46 (d, *J* = 8 Hz, 2H, 4-chlorophenyl-$C_{2,6}$-H), 7.51 (s, 2H, NH_2, D_2O exchangeable), 7.69 (d, *J* = 8 Hz, 2H, 4-chlorophenyl-$C_{3,5}$-H), 8.67 (d, *J* = 2.5 Hz, 1H, pyrazine-C_6-H), 8.70-8.71 (m, 1H, pyrazine-C_5-H), 9.33 (s, 1H, pyrazine-C_3-H), 10.91 (s, 1H, NHCO, D_2O exchangeable). ^{13}C NMR (100 MHz, DMSO-d_6): δ 12.8 (CH_3), 79.6 (dihydrothiazole-C_5), 130.7 (4-chlorophenyl-$C_{3,5}$), 131.5 (4-chlorophenyl-$C_{2,6}$), 134.1 (4-chlorophenyl-C_1), 135.3 (4-chlorophenyl-C_4), 142.9 (pyrazine-C_3), 144.0 (pyrazine-C_6), 144.5 (pyrazine-C_5), 147.6 (C=N) 150.7 (pyrazine-C_2), 155.0 (dihydrothiazole-C_4), 163.6 (C=O), 190.1 (C=S). EI-MS: m/z (406.06) ($M^{+\bullet}$ +2), (404.06) ($M^{+\bullet}$). Anal. Calcd (%) for $C_{16}H_{13}ClN_6OS_2$ (404.9): C, 47.46; H, 3.24; N, 20.76; S, 15.84. Found: C, 47.80; H, 3.18; N, 21.03; S, 15.96.

4.1.5.4. 4-Amino-3-(4-fluorophenyl)-N'-(1-(pyrazin-2-yl)ethylidene)-2-thioxo-2,3-dihydrothiazole-5-carbohydrazide **(12d).**

Yellowish brown crystals, yield 71%. m.p.260~262 °C. IR (KBr, cm^{-1}): 3464.15 (enolic OH), 3356.14, 3232.70, 3159.40 (NH), 1620.21 (C=O), 1508.33 (C=N),

1242.16 (C=S). ^{1}H NMR (400 MHz, DMSO-d_6): δ 2.39 (s, 3H, CH_3), 7.44-7.51 (m, 6H, 4-fluorophenyl-$C_{2,3,5,6}$-H and NH_2, D2O exchangeable), 8.68 (d, *J* = 4 Hz, 1H, pyrazine-C_6-H), 8.69-8.70 (m, 1H, pyrazine-C_5-H), 9.33 (s, 1H, pyrazine-C_3-H), 10.90 (s, 1H, NHCO, D_2O exchangeable). Anal. Calcd (%) for $C_{16}H_{13}FN_6OS_2$ (388.44): C, 49.47; H, 3.37; N, 21.64; S, 16.51. Found: C, 49.71; H, 3.26; N, 21.98; S, 16.60.

4.1.5.5. 4-Amino-3-(4-methoxyphenyl)-N'-(1-(pyrazin-2-yl)ethylidene)-2-thioxo-2,3-dihydrothiazole-5-carbohydrazide **(12e).**

Yellow crystals, yield 68%. m.p.254~256 °C. IR (KBr, cm^{-1}): 3419.33 (enolic OH), 3356.20, 3232.61, 3157.15 (NH), 1623.33 (C=O), 1507.64 (C=N), 1244.12 (C=S). ^{1}H NMR (500 MHz, DMSO-d_6): δ 2.34 (s, 3H, CH_3), 3.81 (s,3H, OCH_3), 7.12 (d, *J* = 10 Hz, 2H, 4-methoxyphenyl-$C_{2,6}$-H), 7.28 (d, *J* =5 Hz, 2H, 4-methoxyphenyl-$C_{3,5}$-H), 7.36 (s, 2H, NH_2, D_2O exchangeable), 8.63 (d, *J* = 3 Hz, 1H, pyrazine-C_6-H), 8.66-8.67 (m, 1H, pyrazine-C_5-H), 9.30 (s, 1H, pyrazine-C_3-H), 10.87 (s, 1H, NHCO, D_2O exchangeable). ^{13}C NMR (100 MHz, DMSO-d_6): δ12.7 (CH_3), 55.95 (OCH_3), 79.4 (thiazole–C_5), 115.7 (4-methoxyphenyl–$C_{3,5}$), 127.6 (4-methoxyphenyl–C_1), 130.6 (4-methoxyphenyl–$C_{2,6}$), 142.9 (pyrazine–C_3), 144.0 (pyrazine–C_6), 144.5 (pyrazine–C_5), 147.5 (C=N), 150.7 (pyrazine–C_2), 155.4 (thiazole–C_4), 160.6 (4-methoxyphenyl–C_4), 163.6 (C=O), 190.5 (C=S). EI-MS: m/z (400.12) ($M^{+\bullet}$). Anal. Calcd (%) for $C_{17}H_{16}N_6O_2S_2$ (400.48): C, 50.98; H, 4.03; N, 20.98; S, 16.01. Found: C, 51.24; H, 3.96; N, 21.26; S, 16.14.

4.1.6. General procedure for synthesis of compounds 13a-e:

A suspension of the appropriate thioxothiophene carbohydrazide **12a-e** (1 mmol) in a mixture of triethylorthoformate and acetic anhydride 1:1 (4 ml) was heated under reflux for 3 h. The mixture was allowed to cool then poured onto crushed ice and refrigerated

overnight. The product formed was filtered, washed with water, dried and crystallized from ethanol.

4.1.6.1. 3-Allyl-6-((1-(pyrazin-2-yl)ethylidene)amino)-2-thioxo-2,3-dihydrothiazolo[4,5-d]pyrimidin-7(6*H*)-one **(13a)**.

Pale brown crystals, yield 80%. m.p.174~176 °C. IR (KBr, cm^{-1}): 1693.50 (C=O), 1577.77 (C=N), 1269.16 (C=S). ^{1}H NMR (400 MHz, DMSO-d_6): δ 2.38 (s, 3H, CH_3), 4.96 (d, *J* = 4 Hz, 2H, $C\underline{H}_2$ –CH=CH_2), 5.14, 5.23 (2d, *J* = 16 Hz, 8 Hz, 2H, CH_2–CH=$C\underline{H}_2$), 5.92-5.99 (m, 1H, CH_2–$C\underline{H}$=CH_2), 8.71 (s, 1H, thiazolopyrimidinone-C_5-H), 8.86-8.87 (m, 1H, pyrazine-C_6-H), 8.91 (d, *J* = 2 Hz, 1H, pyrazine-C_5-H), 9.38 (s, 1H, pyrazine-C_3-H). Anal. Calcd (%) for $C_{14}H_{12}N_6OS_2$ (344.41): C, 48.82; H, 3.51; N, 24.40; S, 18.62. Found: C, 48.97; H, 3.66; N, 24.18; S, 18.70.

4.1.6.2. 3-Phenyl-6-((1-(pyrazin-2-yl)ethylidene)amino)-2-thioxo-2,3-dihydrothiazolo[4,5-d]pyrimidin-7(6*H*)-one **(13b).**

Brown crystals, yield 80%. m.p.250~252 °C. IR (KBr, cm^{-1}): 1685.79 (C=O), 1573.91 (C=N), 1242.16 (C=S). ^{1}H NMR (400 MHz, DMSO-d_6): δ 2.38(s, 3H, CH_3), 7.49 (d, *J* = 8 Hz, 2H, phenyl-$C_{2,6}$-H), 7.57-7.65 (m, 3H, phenyl-$C_{3,4,5}$-H), 8.54 (s, 1H, thiazolopyrimidinone-C_5-H), 8.86-8.87 (m, 1H, pyrazine-C_6-H), 8.90 (d, *J* = 4 Hz, 1H, pyrazine-C_5-H), 9.38 (s, 1H, pyrazine-C_3-H). Anal. Calcd (%) for $C_{17}H_{12}N_6OS_2$ (380.45): C, 53.67; H, 3.18; N, 22.09; S, 16.86. Found: C, 53.41; H, 3.31; N, 21.88; S, 17.02.

4.1.6.3. 3-(4-Chlorophenyl)-6-((1-(pyrazin-2-yl)ethylidene)amino)-2-thioxo-2,3-dihydrothiazolo[4,5-d]pyrimidin-7(6*H*)-one **(13c).**

Brown crystals, yield 95%. m.p.213~215 °C. IR (KBr, cm^{-1}): 1685.79 (C=O), 1570.06 (C=N), 1253.73 (C=S). ^{1}H NMR (400 MHz, DMSO-d_6): δ 2.38 (s, 3H, CH_3), 7.55 (d, *J* = 8 Hz, 2H, 4-chlorophenyl-$C_{2,6}$-H), 7.71 (d, *J* = 8 Hz, 2H, 4-chlorophenyl-$C_{3,5}$-H), 8.56 (s, 1H, thiazolopyrimidinone-C_5-H), 8.86-8.87 (m, 1H, pyrazine-C_6-H), 8.90 (d, *J* = 4 Hz, 1H,

pyrazine-C_5-H), 9.38 (s, 1H, pyrazine-C_3-H). EI-MS: m/z (416.06) ($M^{+\bullet}$ +2), (414.06) ($M^{+\bullet}$). Anal. Calcd (%) for $C_{17}H_{11}ClN_6OS_2$ (414.89): C, 49.21; H, 2.67; N, 20.26; S,15.46. Found: C, 49.54; H, 2.72; N, 19.94; S,15.67.

4.1.6.4. 3-(4-Fluorophenyl)-6-((1-(pyrazin-2-yl)ethylidene)amino)-2-thioxo-2,3-dihydrothiazolo [4,5-d]pyrimidin-7(6*H*)-one **(13d).**

Brown crystals, yield 84%. m.p.209~211 °C. IR (KBr, cm^{-1}): 1685.79 (C=O),

1573.91 (C=N), 1246.02 (C=S). ^{1}H NMR (400 MHz, DMSO-d_6): δ 2.38 (s, 3H, CH_3), 7.45-7.59 (m, 4H, 4-fluorophenyl-$C_{2,3,5,6}$-H), 8.56 (s, 1H, thiazolopyrimidinone-C_5-H), 8.86-8.87 (m, 1H, pyrazine-C_6-H), 8.90 (d, *J* = 2.4 Hz, 1H, pyrazine-C_5-H), 9.38 (s, 1H, pyrazine-C_3-H).^{13}C NMR (100 MHz, DMSO-d_6): δ16.7 (CH_3), 107.3 (thiazolopyrimidinone–C_{7a}), 116.8 (4-fluorophenyl–C_3), 117.0 (4-fluorophenyl–C_5), 131.6 (4-fluorophenyl–$C_{2,6}$), 132.1 (4-fluorophenyl–C_1), 143.7 (pyrazine–C_3), 144.7 (pyrazine–C_6), 147.7 (pyrazine–C_5), 148.3 (C=N), 148.6 (pyrazine–C_2), 149.7 (thiazolopyrimidinone–C_{3a}), 155.8 (thiazolopyrimidinone–C_5), 161.5 (4-fluorophenyl–C_4), 178.6 (C=O), 190.2 (C=S). Anal. Calcd (%) for $C_{17}H_{11}FN_6OS_2$ (398.44): C, 51.25; H, 2.78; N, 21.09; S, 16.1. Found: C, 51.54; H, 2.69; N, 21.38; S, 15.89.

4.1.6.5. 3-(4-Methoxyphenyl)-6-((1-(pyrazin-2-yl)ethylidene)amino)-2-thioxo-2,3-dihydrothiazolo[4,5-d]pyrimidin-7(6*H*)-one **(13e).**

Brown crystals, yield 75%. m.p.162~164 °C. IR (KBr, cm^{-1}): 1685.79 (C=O), 1573.91 (C=N), 1253.73 (C=S). ^{1}H NMR (400 MHz, DMSO-d_6): δ 2.38 (s, 3H, CH_3), 3.86 (s, 3H, OCH_3), 7.14 (d, *J* = 12 Hz, 2H, 4-methoxyphenyl-$C_{2,6}$-H), 7.39 (d, *J* = 12 Hz, 2H, 4-methoxyphenyl-$C_{3,5}$-H), 8.54 (s, 1H, thiazolopyrimidinone-C_5-H), 8.86-8.87 (m, 1H, pyrazine-C_6-H), 8.90 (d, *J* = 4 Hz, 1H, pyrazine-C_5-H), 9.38 (s, 1H, pyrazine-C_3-H). EI-MS: m/z (410.11) ($M^{+\bullet}$). Anal. Calcd (%) for $C_{18}H_{14}N_6O_2S_2$ (410.47): C, 52.67; H, 3.44; N, 20.47; S, 15.62. Found: C, 52.56; H, 3.59; N, 20.63; S, 15.74.

4.1.7. General procedure for synthesis of (*E*)-3-Aryl-1-(pyrazin-2-yl)prop-2-en-1-ones (14a,b):

A mixture of the appropriate aldehyde (1 mmol) and 2-acetylpyrazine **(2)** (1mmol, 0.12 g) and piperidine (2 mmol, 0.2 ml) was heated to fusion at 85°C for 1 h, to the red melt were added ethanol (1.5 ml), glacial acetic acid (0.5 ml) and water to precipitate the product. The product was filtered off, washed with ethanol, dried and crystallized from ethanol. In case of 2-thiophen carbaldehyde, the product obtained was a sticky mass which was triturated with diethyl ether then petroleum ether to afford a yellow precipitate, which was crystallized from ethanol.

4.1.7.1. (*E*)-3-(3,4-Dimethoxyphenyl)-1-(pyrazin-2-yl)prop-2-en-1-one **(14a).**

Yellow crystals, yield 50%. m.p.120~122 °C. IR (KBr, cm^{-1}): 1661.35 (C=O), 1576.76 (C=N), 1262.86,1061.41 (C–O–C). ^{1}H NMR (400 MHz, $CDCl_3$): δ 3.96, 3.99 (2s, each 3H, $2OCH_3$), 6.93 (d, *J* = 8 Hz, 1H, CO – C<u>H</u> = CH), 7.27-7.95 (m, 2H, 3,4-dimethoxyphenyl-$C_{5,6}$-H), 7.95-8.07 (m, 2H, CO – CH = C<u>H</u> and 3,4-dimethoxyphenyl-C_2-H), 8.72-8.73 (m, 1H, pyrazine-C_6-H), 8.79 (d, *J* = 2 Hz, 1H, pyrazine-C_5-H), 9.39 (s, 1H, pyrazine-C_3-H). EI-MS: m/z (270.17) ($M^{+\bullet}$). Anal. Calcd (%) for $C_{15}H_{14}N_2O_3$ (270.28): C, 66.66; H, 5.22; N, 10.36. Found: C, 66.90; H, 5.20; N, 10.54.

4.1.7.2. (*E*)-1-(Pyrazin-2-yl)-3-(thiophen-2-yl)prop-2-en-1-one **(14b).**

Yellow powder, yield 77%. m.p.118~120 °C. IR (KBr, cm^{-1}): 1662.64 (C=O), 1589.34 (C=N). ^{1}H NMR (400 MHz, DMSO-d_6): δ 7.27 (t, *J* = 4 Hz, 1H, 2-thienyl-C_4-H), 7.76 (d, *J* = 4 Hz, 1H, 2-thienyl-C_5-H), 7.86, 7.89 (2d, *J* = 4 Hz, 16 Hz, 2H, 2-thienyl-C_3-H and CO – C<u>H</u> = CH), 8.14 (d, *J* = 16 Hz, 1H, CO – CH = C<u>H</u>), 8.90-8.91 (m, 1H, pyrazine-C_6-H), 8.97 (d, *J* = 4 Hz, 1H, pyrazine-C_5-H), 9.28 (s, 1H, pyrazine-C_3-H). EI-MS: m/z (216.10) ($M^{+\bullet}$). Anal. Calcd (%) for $C_{11}H_8N_2OS$ (216.26): C, 61.09; H, 3.73; N, 12.95; S, 14.83. Found: C, 61.24; H, 3.81; N, 13.17; S, 14.78.

4.1.8. 2-[5-(3,4-Dimethoxyphenyl)-4,5-dihydro-1*H*-pyrazol-3-yl]pyrazine **(15a).**

A solution of the chalcone **14a** (1 mmol, 0.27 g), and hydrazine hydrate 99% (1.1 mmol, 0.06 gm, 0.06 ml) in absolute ethanol (2 ml) was refluxed for 10 h. The reaction mixture was left to cool and refrigerated overnight. The crystalline product obtained was filtered off, washed with ethanol, dried and recrystallized from ethanol.

White powder, yield 53%. m.p.110~112 °C. IR (KBr, cm^{-1}): 3305.99 (NH), 1593.20 (C=N), 1141.86, 1022.27 (C–O –C). ^{1}H NMR (400 MHz, DMSO-d_6): δ 2.91 (dd, J_{ab} = 16.8 Hz, J_{ax} = 10.8 Hz, 1H, Ha, pyrazoline-C_4-H), 3.48 (dd, J_{ax} = 16.8 Hz, J_{bx} = 11.32 Hz, 1H, Hx, pyrazoline-C_5-H), 3.73,3.75 (2s, each 3H, 2 OCH_3), 4.90 (t, J = 11 Hz, 1H, Hb, pyrazoline-C_4-H), 6.87-6.93 (m, 2H, phenyl-$C_{5,6}$-H), 6.98 (s, 1H, phenyl-C_2-H), 8.24 (s, 1H, NH,D_2O exchangeable), 8.47, 8.55 (2s, 2H, pyrazine-$C_{5,6}$-H), 9.10 (s, 1H, pyrazine-C_3-H). EI-MS: m/z (284.17) ($M^{+\bullet}$). Anal. Calcd (%) for $C_{15}H_{16}N_4O_2$ (284.31): C, 63.37; H, 5.67; N, 19.71. Found: C, 63.54; H, 5.78; N, 19.97.

4.1.9. 2-[5-(3,4-Dimethoxyphenyl)-1-phenyl-4,5-dihydro-1*H*-pyrazol-3-yl]pyrazine **(15b).**

A solution of the chalcone **14a** (1 mmol, 0.27 g), and phenyl hydrazine (2 mmol, 0.3 ml) in absolute ethanol (5 ml) was refluxed for 4 h. The resulting solution was left to cool. The crystalline product obtained was filtered off, washed with ethanol, dried and recrystallized from ethanol.

Yellow crystals, yield 50%. m.p.160~162 °C. IR (KBr, cm^{-1}): 2987.12 (Ar – H), 2924.16 (Aliph – H), 1593.22 (C=N), 1160.62, 1017.56 (C – O – C). ^{1}H NMR (400 MHz, DMSO-d_6): δ 3.14 (dd, J_{ab} = 17.88 Hz, J_{ax} = 6.56 Hz, 1H, Ha, pyrazoline-C_4-H), 3.70,3.71 (2s, each 3H, 2 OCH_3), 3.92 (dd, J_{ba} = 17.92 Hz, J_{bx} = 12.56 Hz, 1H, Hb, pyrazoline-C_4-H), 5.52 (dd, J_{ax} = 6.60 Hz, J_{bx} = 12.52 Hz, 1H, Hx, pyrazoline-C_5-H), 6.75-7.22 (m, 8H, 3,4-dimethoxyphenyl-$C_{2,5,6}$-H and phenyl-$C_{2,3,4,5,6}$-H), 8.52 (d, J = 4 Hz, 1H, pyrazine-C_6-H), 8.59-8.60 (m, 1H, pyrazine-C_5-H), 9.30 (s, 1H, pyrazine-C_3-H).^{13}C NMR (100 MHz, DMSO-d_6): δ 42.7 (pyrazoline-C_4), 55.8 (pyrazoline-C_5), 56.5 (OCH_3), 63.6 (OCH_3), 110.1 (3,4-dimethoxyphenyl-C_2), 111.9 (phenyl-$C_{2,6}$), 114.0 (3,4-dimethoxyphenyl-C_6), 118.2 (phenyl-C_4), 120.1 (3,4-dimethoxyphenyl-C_5), 129.6 (phenyl-$C_{3,5}$), 134.7 (3,4-

dimethoxyphenyl-C_1), 142.5 (pyrazine-C_3), 143.3 (pyrazine-C_6), 143.9 (phenyl-C_1), 144.4 (pyrazine-C_5), 146.3 (3,4-dimethoxyphenyl-C_4), 147.7 (3,4-dimethoxyphenyl-C_3), 148.5 (pyrazine-C_2), 149.5 (pyrazoline-C_3). EI-MS: m/z (360.21) ($M^{+\bullet}$). Anal. Calcd (%) for $C_{21}H_{20}N_4O_2$ (360.41): C, 69.98; H, 5.59; N, 15.55. Found: C, 70.23; H, 5.64; N, 15.80.

4.1.10. 1-[5-(3,4-Dimethoxyphenyl)-3-(pyrazin-2-yl)-4,5-dihydro-1*H*-pyrazol-1-yl]ethanone **(16).**

A solution of the chalcone 14a (1 mmol, 0.27 g), and hydrazine hydrate 99% (1.1 mmol, 0.06 g, 0.06 ml) in 96% acetic acid (2 ml) was refluxed for 16 h. The resulting red solution was left to cool and the solvent was evaporated to dryness. The red crystalline product obtained was filtered off, washed with petroleum ether, dried and recrystallized from benzene.

Brick red crystals, quantitative yield. m.p.125~127 °C. IR (KBr, cm^{-1}): 1693.50 (C=O), 1597.06 (C=N), 1261.45, 1014.56 (C – O – C). ^{1}H NMR (400 MHz, DMSO-d_6): δ 2.35 (s, 3H, CH_3), 3.15 (dd, J_{ab} = 18.52 Hz, J_{ax} = 4.84 Hz,1H, Ha, pyrazoline-C_4-H), 3.72, 3.73 (2s, each 3H, 2 OCH_3), 3.83-3.92 (m, 1H, Hb, pyrazoline-C_4-H), 5.52 (d, *J* = 11.84 Hz, 1H, Hx, pyrazoline-C_5-H), 6.69 (d, *J* = 8 Hz, 1H, 3,4-dimethoxyphenyl-C_6-H), 6.83 (s, 1H,3,4-dimethoxyphenyl-C_2-H), 6.87 (d, *J* = 8 Hz, 1H, 3,4-dimethoxyphenyl-C_5-H), 8.60-8.80 (m, 2H, pyrazine-$C_{5,6}$-H), 9.27(s,1H, pyrazine-C_3-H). Anal. Calcd (%) for $C_{17}H_{18}N_4O_3$ (326.35): C, 62.57; H, 5.56; N, 17.71. Found: C, 62.84; H, 5.50; N, 17.43.

4.1.11. 5-(3,4-Dimethoxyphenyl)-3-(pyrazin-2-yl)isoxazole **(17).**

A solution of 14a (1 mmol, 0.27 g), hydroxylamine hydrochloride (1.4 mmol, 0.1 g) and a catalytic amount of glacical acetic acid (0.5 ml) in absolute ethanol (10 ml), was heated under reflux for 10 h, then the mixture was poured onto crushed ice. The orange precipitate separated was filtered off, washed with water, dried and crystallized from ethanol.

Orange crystals, yield 48%. m.p.204~206 °C. IR (KBr, cm^{-1}): 1557.25 (C=N), 1256.40, 1010.70 (C – O – C). ^{1}H NMR (400 MHz, DMSO-d_6): δ 3.85, 3.86 (2s, each 3H, 2 OCH_3); 6.88 (s, 1H, isoxazole-C_4-H); 7.14-7.29 (m, 3H, 3,4-dimethoxyphenyl-$C_{2,5,6}$-H); 8.22 (d, *J* = 8 Hz, 2H, pyrazine-$C_{5,6}$-H); 9.25 (s, 1H, pyrazine-C_3-H). EI-MS: m/z (283.92) ($M^{+\bullet}$). Anal. Calcd (%) for $C_{15}H_{13}N_3O_3$ (283.28): C, 63.6; H, 4.63; N, 14.83. Found: C, 63.49; H, 4.75; N, 14.40.

4.1.12. 5-(3,4-Dimethoxyphenyl)-3-(pyrazin-2-yl)-4,5-dihydro-1*H*-pyrazole-1-carbothioamide **(18).**

A mixture of 14a (1 mmol, 0.27 g), thiosemicarbazide (2.2 mmol, 0.2 g) and sodium hydroxide (0.5 mmol, 0.03 g) in absolute ethanol (5ml) was refluxed for 12 h. The reaction mixture was left to cool to room temperature then poured onto ice/water mixture and few drops of hydrochloric acid (2 drops) were added. A yellow crystalline product was obtained, filtered off, washed with petroleum ether, dried and recrystallized from ethanol/water.

Yellow crystals, yield 52%. m.p.183~185 °C. IR (KBr, cm^{-1}): 3417.86, 3278.99 (NH_2), 1589.34 (C=N), 1141.86 (C=S). ^{1}H NMR (400 MHz, DMSO-d_6): δ 3.13 (dd, J_{ax} = 18.44 Hz, J_{ab} = 3.40 Hz, 1H, Ha, pyrazoline-C_4-H), 3.71 (s, 6H, 2OCH_3), 3.91 (dd, J_{ax} = 18.44 Hz, J_{bx} = 11.44 Hz,1H, Hx pyrazoline-C_5-H), 5.89 (d, *J* = 11.44 Hz, 1H, Hb, pyrazoline-C_4-H), 6.61 (d, *J* = 8 Hz, 1H, 3,4-dimethoxyphenyl-C_6-H), 6.80 (s, 1H, 3,4-dimethoxyphenyl-C_2-H), 6.86 (d, *J* = 8 Hz, 1H, 3,4-dimethoxyphenyl-C_5-H), 8.16, 8.26 (2s, 2H, NH_2, D_2O exchangeable), 8.66 (d, *J* = 5.6 Hz, 2H, pyrazine-$C_{5,6}$-H), 9.51(s,1H, pyrazine-C_3-H). ^{13}C NMR (100 MHz, DMSO-d_6): δ 42.5 (pyrazoline-C_4), 55.9 (2 OCH_3), 63.3 (pyrazoline-C_5), 110.1 (3,4-dimethoxyphenyl-C_2), 112.2 (3,4-dimethoxyphenyl-C_6), 117.5 (3,4-dimethoxyphenyl-C_5), 135.6 (3,4-dimethoxyphenyl-C_1), 143.9 (pyrazine-C_3), 144.6 (pyrazine-C_6), 145.3 (pyrazine-C_5), 146.5 (3,4-dimethoxyphenyl-C_4), 148.2 (3,4-dimethoxyphenyl-C_3), 149.1 (pyrazine-C_2), 154.0 (pyrazoline-C_3), 177.4 (C=S). EI-MS: m/z (343.04) ($M^{+\bullet}$). Anal. Calcd (%) for $C_{16}H_{17}N_5O_2S$ (343.40): C, 55.96; H, 4.99; N, 20.39; S, 9.34. Found: C, 56.15; H, 5.07; N, 20.51; S,9.49.

4.1.13. 2-[5-(3,4-Dimethoxyphenyl)-3-(pyrazin-2-yl)-4,5-dihydro-1*H*-pyrazol-1-yl]-4-phenylthiazole **(19).**

A mixture of compound 18 (1 mmol, 0.34 g), and phenacyl bromide (1 mmol, 0.2 g) in absolute ethanol (4 ml) was refluxed for 6 h. The reaction mixture was left to cool to room temperature. The product obtained was filtered off, washed with ethanol, dried and crystallized from benzene.

Dark red crystals, yield 50%. m.p.164~166 °C. IR (KBr, cm^{-1}): 3047.53 (Ar – H), 1593.20 (C=N), 1138.00, 1026.13 (C – O– C). ^{1}H NMR (400 MHz, DMSO-d_6): δ 3.43 (dd, J_{ba} = 18.32 Hz, J_{bx} = 6.88 Hz, 1H, Ha, pyrazoline-C_4-H), 3.71, 3.77 (2s, each 3H, 2OCH_3), 4.08 (dd, J_{ab} = 18.32 Hz, J_{ax} = 12.16 Hz,1H, Hb, pyrazoline-C_4-H), 5.69 (dd, J_{ax}= 12.20 Hz, J_{bx} = 6.96 Hz,1H, Hx, pyrazoline-C_5-H), 6.90-6.96 (m, 2H, 3,4-dimethoxyphenyl-$C_{5,6}$-H), 7.12 (s, 1H, 3,4-dimethoxyphenyl-C_2-H), 7.26-7.30 (m, 1H,phenyl-C_4-H), 7.35-7.39 (m, 2H, phenyl-$C_{3,5}$-H), 7.41 (s, 1H, thiazole-C_5-H), 7.78 (d, *J* = 8 Hz, 2H, phenyl-$C_{2,6}$-H), 8.66 (d, *J* = 4 Hz, 1H, pyrazine-C_6-H), 8.71-8.72 (m, 1H, pyrazine-C_5-H), 9.24 (s, 1H, pyrazine-C_3-H). EI-MS: m/z (443.07) ($M^{+\bullet}$). Anal. Calcd (%) for $C_{24}H_{21}N_5O_2$ S (443.52): C, 64.99; H, 4.77; N, 15.79; S, 7.23. Found: C, 65.34; H, 4.81; N, 16.04; S,7.41.

4.1.14. 4-(3,4-Dimethoxyphenyl)-6-(pyrazin-2-yl)pyrimidin-2(1*H*)-one **(20).**

To a solution of urea (2 mmol, 0.12 g) in ethanol (4ml) and hydrochloric acid (1.5ml), compound **14a** (1 mmol, 0.27 g) was added and the reaction mixture was heated under reflux for 6 h, during which the solution turns red. After being cooled to room temperature, the mixture was neutralized with dilute ammonia solution (10%) and set aside in refrigerator for 2 h. The product obtained was filtered off, washed with diethyl ether and crystallized from ethanol.

Red crystals, yield 55%. m.p.180~182 °C. IR (KBr, cm^{-1}): 3441.01, 3387.00 (NH), 1643.35 (amide C=O), 1253.73, 1014.86 (C – O – C). ^{1}H NMR (400 MHz, DMSO-d_6): δ 3.83, 3.84 (2s, each 3H, 2 OCH_3), 6.66 (s, 1H, pyrimidinone-C_5-H), 7.10,7.13 (2s, 1H, tautomerized pyrimidinone NH, D_2O exchangeable), 7.17-7.21 (m, 3H, 3,4-dimethoxyphenyl-$C_{2,5,6}$-H),

8.09 (d, *J*= 4 Hz, 2H, pyrazine-$C_{5,6}$-H), 8.89 (s, 1H, pyrazine-C_3-H). EI-MS: m/z (310.97) ($M^{+\bullet}$). Anal. Calcd (%) for $C_{16}H_{14}N_4O_3$ (310.31): C, 61.93; H, 4.55; N, 18.06. Found: C, 61.78; H, 5.24; N, 18.20.

4.1.15. 4-(3,4-Dimethoxyphenyl)-6-(pyrazin-2-yl)pyrimidine-2(1*H*)-thione **(21).**

A mixture of chalcone 14a (1 mmol, 0.27 g), thiourea (1 mmol, 0.08 g) and anhydrous potassium carbonate (1 mmol, 0.14 g) in ethanol (10 ml) was heated under reflux for 12 h, then allowed to cool to room temperature. The product obtained was filtered and washed with ethanol. The product was then suspended in water and neutralized with dilute hydrochloric acid (0.5 ml in 10 ml water). The yellow product obtained was filtered off, washed with water, dried and crystallized from ethanol.

yellow crystals, yield 63%. m.p.209~211 °C. IR (KBr, cm^{-1}): 3406.29 (NH), 2603 (SH), 1581.63 (C=N), 1265.30, 1080.14 (C – O – C), 1149.57 (C=S). ^{1}H NMR (400 MHz, DMSO-d_6): δ 3.63, 3.81, 3.86, 3.90 (4s, 6H, 2 OCH_3, thione &thiol tautomers), 6.99-7.14 (m, 1H, 3,4-dimethoxyphenyl-C_5-H), 7.63-7.95 (m, 2H, 3,4-dimethoxyphenyl-$C_{2,6}$-H), 8.47 (s, 1H, pyrimidin-2-thione-C_5-H), 8.63 (s, 1H, NH, D_2O exchangeable), 8.82-8.89 (m, 2H, pyrazine-$C_{5,6}$-H), 9.41,9.52 (2s, 1H, pyrazine-C_3-H, thione &thiol tautomers), 13.32 (s, 1H, SH, D_2O exchangeable). Anal. Calcd (%) for $C_{16}H_{14}N_4O_2S$ (326.37): C, 58.88; H, 4.32; N, 17.17; S, 9.82. Found: C, 58.80; H, 4.79; N, 17.34; S, 9.63.

4.1.16. General procedure for synthesis of compounds 22a,b:

A mixture of 2-acetylpyrazine (2) (1 mmol, 0.12 g), malononitrile (1 mmol, 0.07 g), the appropriate aromatic aldehyde (1 mmol) and ammonium acetate (8 mmol, 0.58 g) was heated under reflux in absolute ethanol (10 ml) for 4 h. The product obtained was filtered off, washed with ethanol and crystallized from the appropriate solvent.

4.1.16.1. 2-Amino-4-(3,4-dimethoxyphenyl)-6-(pyrazin-2-yl)nicotinonitrile **(22a).**

Yellow crystals, cryst. solvent: dioxane, yield 91%. m.p.261~263 °C. IR (KBr, cm^{-1}): 3405.25, 3338.87 (NH), 2211.39 (C≡N), 1552.49 (C=N), 1266.59,1022.77 (C – O –C). ^{1}H

NMR (400 MHz, DMSO-d_6): δ 3.83, 3.84 (2s, each 3H, $2OCH_3$), 6.84 (s, 2H, NH_2, D_2O exchangeable), 7.12 (d, *J* = 8 Hz, 1H, 3,4-dimethoxyphenyl-C_6-H), 7.19 (s, 1H, 3,4-dimethoxyphenyl-C_2-H), 7.24 (d, *J* = 4Hz, 1H, 3,4-dimethoxyphenyl-C_5-H), 7.27(s, 1H, pyridine-C_5-H), 8.80 (d, *J* = 2.48 Hz, 1H, pyrazine-C_6-H), 8.83-8.84 (m, 1H, pyrazine-C_5-H), 9.17 (s, 1H, pyrazine-C_3-H). EI-MS: m/z (333.55) ($M^{+\bullet}$). Anal. Calcd (%) for $C_{18}H_{15}N_5O_2$ (333.34): C, 64.86; H, 4.54; N, 21.01. Found: C, 65.02; H, 4.63; N, 21.28.

4.1.16.2. 2-Amino-6-(pyrazin-2-yl)-4-(thiophen-2-yl)nicotinonitrile **(22b).**

Brown crystals, cryst. solvent: ethanol, yield 50%. m.p.309~311 °C. IR (KBr, cm^{-1}): 3471.87, 3363.86 (NH), 2214.28 (C≡N), 1577.77 (C=N), 1265.30, 1018.41 (C – O –C). ^{1}H NMR (500 MHz, DMSO-d_6): δ 6.91 (s, 2H, NH_2, D_2O exchangeable), 7.23 (s, 1H, pyridine-C_5-H), 7.25 (t, *J* = 5Hz, 1H, thienyl-C_4-H), 7.64 (d, *J* = 3.8 Hz, 1H, thienyl-C_3-H), 7.84 (d, *J* = 5Hz, 1H, thienyl-C_5-H), 8.77-8.80 (m, 2H, pyrazine-$C_{5,6}$-H), 9.12 (s, 1H, pyrazine-C_3-H). EI-MS: m/z (279.10) ($M^{+\bullet}$). Anal. Calcd (%) for $C_{14}H_9N_5S$ (279.32): C, 60.20; H, 3.25; N, 25.07; S, 11.48. Found: C, 60.27; H, 3.35; N, 25.19; S, 11.45.

4.1.17. General procedure for synthesis of compounds 23a,b:

A mixture of 2-acetylpyrazine (2) (2mmol, 0.24 g), ethyl cyanoacetate (2 mmol, 0.21 g, 0.19 ml), the appropriate aldehyde (2 mmol), and ammonium acetate (16 mmol, 1.2 g) was heated under reflux in absolute ethanol (10 ml) for 4 h during which precipitation of the product occurred. The reaction mixture was left to cool to room temperature, the product obtained was filtered, washed with ethanol, dried and crystallized from the appropriate solvent.

4.1.17.1 4-(3,4-Dimethoxyphenyl)-2-oxo-6-(pyrazin-2-yl)-1,2-dihydropyridine-3-carbonitrile **(23a).**

Yellow crystals, cryst. solvent: dioxane, yield 45%. m.p.260~262 °C. IR (KBr, cm^{-1}): 3407.48 (enolic OH), 3291.69 (NH), 2214.92 (C≡N), 1691.36 (amide C=O), 1609.31 (C=N), 1259.47, 1017.10 (C – O – C). ^{1}H NMR (400 MHz, DMSO-d_6): δ 3.86 (s, 6H, $2OCH_3$), 7.06-7.43 (m, 4H, pyridine-C_5-H and 3,4-dimethoxyphenyl-$C_{2,5,6}$-H), 8.82 (brs, 2H, pyrazine-$C_{5,6}$-H), 9.48 (s, 1H, pyrazine-C_3-H), 12.53 (s, 1H, NH, D_2O exchangeable).

Anal. Calcd (%) for $C_{18}H_{14}N_4O_3$ (334.33): C, 64.66; H, 4.22; N, 16.76. Found: C, 64.90; H, 4.38; N, 17.04.

4.1.17.2. 2-Oxo-6-(pyrazin-2-yl)-4-(thiophen-2-yl)-1,2-dihydropyridine-3-carbonitrile **(23b).**

Beige crystals, cryst. solvent: ethanol, yield 41%. m.p.304~306 °C. IR (KBr, cm^{-1}): 3421.72 (enolic OH), 3105.39 (NH), 2222.00 (C≡N), 1680.92 (amide C=O), 1600.92 (C=N), 1253.73, 1018.41 (C – O – C). ^{1}H NMR (500 MHz, DMSO-d_6): δ 7.32 (t, *J* = 5 Hz, 1H, thienyl-C_4-H), 7.52 (s, 1H, pyridine-C_5-H), 8.01 (d, *J* = 5 Hz, 1H, thienyl-C_3-H), 8.07 (d, *J* = 3 Hz, 1H, thienyl-C_5-H), 8.80-8.81 (m, 2H, pyrazine-$C_{5,6}$-H), 9.45 (s, 1H, pyrazine-C_3-H), 12.61 (s, 1H, NH, D_2O exchangeable). ^{13}C NMR (100 MHz, DMSO-d_6): δ 117.0 (pyridin-2-one-C_5), 117.4 (CN), 129.3 (pyridin-2-one-C_3), 132.0 (thienyl-C_3), 132.7 (thienyl-C_4), 137.0 (thienyl-C_5), 143.4 (thienyl-C_2), 143.9 (pyridin-2-one-C_6), 144.5 (pyrazine-C_5), 144.8 (pyrazine-C_3), 146.0 (pyrazine-C_6), 146.9 (pyrazine-C_2), 150.7 (pyridin-2-one-C_4), 154.8 (C=O). EI-MS: m/z (280.08) ($M^{+\bullet}$). Anal. Calcd (%) for $C_{14}H_8N_4OS$ (280.30): C, 59.99; H, 2.88; N, 19.99; S, 11.44. Found: C, 59.65; H, 2.86; N, 20.23; S, 11.41.

4.1.18. General procedure for synthesis of compounds 24a,b:

A mixture of 2-acetylpyrazine (2) (2 mmol, 0.24 g), 2-cyanothioacetamide (2 mmol, 0.2 g), the appropriate aldehyde (2 mmol), and ammonium acetate (16 mmol, 1.2 g), was heated under reflux in absolute ethanol (10 ml) for 8 h during which precipitation of the product occurred. On cooling to room temperature, the product obtained was filtered, washed with ether, dried and crystallized from ethanol.

4.1.18.1. 4-(3,4-Dimethoxyphenyl)-6-(pyrazin-2-yl)-2-thioxo-1,2-dihydropyridine-3-carbonitrile **(24a).**

Red crystals, yield 47%. m.p.234~236 °C. IR (KBr, cm^{-1}): 3182.55 (NH), 2210.42 (C≡N), 1597.06 (C=N), 1149.57 (C=S), 1265.30, 1099.43 (C – O – C). ^{1}H NMR (400 MHz, DMSO-d_6): δ 3.86, 3.87 (2s, each 3H, 2OCH_3), 7.18 (d, *J* = 8 Hz, 1H, 3,4-dimethoxyphenyl-C_5-H), 7.40-7.43 (m, 2H, 3,4-dimethoxyphenyl-C_2,6-H), 7.69 (s,1H,

pyridine-2-thione-C_5-H), 8.88 (brs, 2H, pyrazine-$C_{5,6}$-H), 9.52 (s, 1H, pyrazine-C_3-H), 13.46 (s, 1H, NH, D_2O exchangeable). ^{13}C NMR (100 MHz, DMSO-d_6): δ 56.2 (2 OCH_3), 110.8 (pyridine-2-thione-C_3), 112.4 (pyridine-2-thione-C_5), 113.2 (3,4-dimethoxyphenyl-C_5), 114.3 (3,4-dimethoxyphenyl-C_2), 117.4 (CN), 122.5 (3,4-dimethoxyphenyl-C_6), 127.5 (3,4-dimethoxyphenyl-C_1), 143.3 (pyrazine-C_5), 143.79 (pyrazine-C_3), 146.3 (pyrazine-C_6), 147.3 (3,4-dimethoxyphenyl-C_4), 149.3 (3,4-dimethoxyphenyl-C_3), 151.3 (pyrazine-C_2), 151.6 (pyridine-2-thione-C_6), 156.6 (C=S), 179.5 (pyridine-2-thione-C_4). EI-MS: m/z (350.13) ($M^{+\bullet}$). Anal. Calcd (%) for $C_{18}H_{14}N_4O_2S$ (350.39): C, 61.70; H, 4.03; N, 15.99; S, 9.15. Found: C, 61.96; H, 4.12; N, 16.23; S, 9.28.

4.1.18.2. 6-(Pyrazin-2-yl)-4-(thiophen-2-yl)-2-thioxo-1,2-dihydropyridine-3-carbonitrile **(24b).**

Brown crystals, yield 47%. m.p.225~227 °C. IR (KBr, cm^{-1}): 3282.84 (NH), 2218.14 (C≡N), 1612.49 (C=N), 1157.29 (C=S), 1253.73, 1053.13 (C – O – C). ^{1}H NMR (400 MHz, DMSO-d_6): δ 7.38-8.17 (m, 4H, thienyl-$C_{3,4,5}$-H and pyridine-2-thione-C_5-H), 8.75-8.88 (m, 2H, pyrazine-$C_{5,6}$-H), 9.52 (s, 1H, pyrazine-C_3-H), 13.54 (s, 1H, NH, D_2O exchangeable). Anal. Calcd (%) for $C_{14}H_8N_4S_2$ (296.37): C, 56.74; H, 2.72; N, 18.90; S, 21.64. Found: C, 56.98; H, 2.67; N, 19.23; S, 21.79.

4.1.19. Ethyl 3',4'-dimethoxy-3-oxo-5-(pyrazin-2-yl)-1,2,3,6-tetrahydro-[1,1'-biphenyl]-2-carboxylate **(25).**

A mixture of 2-acetylpyrazine **(2**) (1 mmol, 0.12 g), 3,4-dimethoxybenzaldehyde (1 mmol, 0.16 g), ethyl acetoacetate (1 mmol, 0.13 g, 0.12 ml) and 10% ethanolic sodium hydroxide (0.3 ml) was refluxed for 6 h in absolute ethanol (5 ml). The reaction mixture was left to cool to room temperature and then poured onto ice/water mixture. The product obtained was filtered, washed with water, dried and crystallized from ethanol.

White crystals, yield 50%. m.p.128~130 °C. IR (KBr, cm^{-1}): 1732.08 (ester C=O), 1678.07 (ketone C=O), 1265.30, 1095.57 (C – O – C). ^{1}H NMR (400 MHz, DMSO-d_6): δ 1.06 (t,

J= 6Hz, 3H, $CH_2C\underline{H_3}$), 3.05-3.09 (m, 1H, Ha, cyclohex-3-en-2-one carboxylate-C_5-H), 3.61-3.68 (m, 2H, cyclohex-3-en-2-one carboxylate-C_5-Hb and C_6-H), 3.74, 3.75 (2s, each 3H, $2OCH_3$), 3.95 (q, 2H, $C\underline{H_2}CH_3$), 4.19 (d, *J*=12 Hz, 1H, cyclohex-3-en-2-one carboxylate-C_1-H), 6.90-7.08 (m, 4H, 3,4-dimethoxyphenyl-$C_{2,5,6}$-H and cyclohex-3-en-2-one carboxylate-C_3-H), 8.71 (d, *J* = 4 Hz, 1H, pyrazine-C_6-H), 8.73-8.75 (m, 1H, pyrazine-C_5-H), 9.21 (s, 1H, pyrazine-C_3-H). ^{13}C NMR (100 MHz, DMSO-*d*$_6$): δ 14.3 ($CH_2\underline{C}H_3$), 33.9 (cyclohex-3-en-2-one carboxylate-C_6), 43.7 (cyclohex-3-en-2-one carboxylate-C_5), 56.0 (2 OCH_3), 59.7 ($\underline{C}H_2CH_3$), 60.9 (cyclohex-3-en-2-one carboxylate-C_1), 111.7 (3,4-dimethoxyphenyl-C_2), 112.2 (3,4-dimethoxyphenyl-C_5), 119.6 (3,4-dimethoxyphenyl-C_6), 125.8 (cyclohex-3-en-2-one carboxylate-C_3), 134.4 (pyrazine-C_5), 143.6 (3,4-dimethoxyphenyl-C_1), 144.7 (pyrazine-C_3), 145.7 (3,4-dimethoxyphenyl-C_4), 148.0 (pyrazine-C_6), 149.0 (3,4-dimethoxyphenyl-C_3), 150.0 (pyrazine-C_2), 169.6 (cyclohex-3-en-2-one carboxylate-C_4), 195.3 (C=O ester), 199.3 (C=O ketone). EI-MS: m/z (382.87) ($M^{+\bullet}$). Anal. Calcd (%) for $C_{21}H_{22}N_2O_5$ (382.41): C, 65.96; H, 5.80; N, 7.33. Found: C, 66.24; H, 5.75; N, 7.29.

4.2. Biological evaluation

4.2.1. *In vitro* anti-mycobacterial assay against H_{37}RV

Microplate alamar blue assay (MABA) was used to determine MICs of the test compounds against *Mtb* using PZA, INH and EMB as reference drugs. Preparation of the inoculum was done using fresh Lowenstein-Jensen (LJ) medium re-suspended in 7H9-S medium (7H9 broth, 0.1% casitone, 0.5% glycerol, supplemented oleic acid, albumin, dextrose, and catalase (OADC)), adjusted to a McFarland tube No. 1, and diluted 1:20; 100 µl was used as inoculum. Tested compounds were dissolved in DMSO. Drug-free controls containing broth with DMSO were included in the experiment. The final concentration of DMSO in the test medium did not exceed 0.5% (*v*/*v*) of the total solution composition, which had no effect on the growth of mycobacteria. Stock solution of each drug was thawed and diluted in 7H9-S at four-fold the final highest concentration tested. The 96 plates were treated with 100 µl 7H9-S and two-fold serial dilution of each compound was made directly on the plate. Final concentrations of the tested compounds in wells were 100, 50, 25, 12.5, 6.25, 3.12, 1.56 and 0.78 µg/mL. Sterile deionized water (200 µl) was

added to all outer-perimeter wells of sterile 96 well plates to decrease evaporation of the medium in the test wells during incubation. A growth control without antibiotic and a sterile control were also set on each plate. The plate was then covered, sealed in plastic bags and incubated at 37^{o}C in normal atmosphere. After 7 days of incubation, each well was supplied with 30 ml of alamar blue solution, and the plate was re-incubated overnight. Colour change from blue (oxidised state) to pink (reduced) highlighted the growth of bacteria, and the MIC was expressed as the minimum concentration of compound which prohibited blue to pink colour change. MIC values were calculated in µg/ml.

4.2.2. *In vitro* cytotoxicity assay

The cytotoxicity of the most active compounds **(8a-d, 14b and 18)** was assessed by microculture tetrazolium (MTT) assay against peripheral blood mononuclear cells (PBMCs). Cytotoxicity testing involved isolation and cultivation of cells, followed by incubation with test samples and finally, measuring cell viability.

4.2.2.1. Human peripheral blood mononuclear cells isolation and culture conditions

PBMCs were isolated from heparinized peripheral blood (as a generous supply from Alexandria University hospital) using a density gradient centrifugation technique described by Boyum [82, 83]. Blood samples were freshly gathered into heparinized sterile tubes. Diluted blood was layered over an equal volume of Ficoll-Paque^{TM} PLUS (Amersham Biosciences) (density 1.077 g/l) (lymphocyte Separation Medium (LSM)) and centrifuged at 1800 rpm for 30 minutes with no acceleration and break at room temperature. The buffy mononuclear cell layer was collected into 15 ml sterile Falcon tube using sterile Pasteur pipette and washed twice in 10 ml phosphate-buffered saline (PBS) pH 7.4 by centrifugation at 1650 rpm for 5 minutes. Evaluation of the viability of isolated PBMCs was done by Trypan blue exclusion method [84]. PBMCs were resuspended at 1 x 10^{6} cells/ml in Rosewell Park Memorial Institute RPMI-1640 medium (Euroclone, Italy) containing 25 mM 4-(2-hydroxyethyl)-1-piperazine-ethanesulfonic acid (HEPES) and 4 mM L-Glutamine (Lonza, Switzerland) supplied with 10% heat-inactivated fetal bovine serum (FBS) (Euroclone, Italy).

4.2.2.2. Incubation with test samples

Test compounds were serially diluted in a 96-well plate. Cell suspension at 1 x 10^6 cells/ml (final cell number/well was equal to 1×10^5 cells in 100 µl culture media) was added to the test formulations (100 µl/well). Control wells were prepared by adding 100 µl culture media to a suspension of 1×10^5 cells in 100 µl culture media. Each set of samples was pipetted in triplicate. The plate was tenderly shaken then incubated at 37 ºC, 5% CO_2 for 24 hours.

4.2.2.3. Microculture tetrazolium (MTT) assay

The viability of cells was determined by the colorimetric 3-[4,5-dimethyl-2-thiazolyl]-2,5-diphenyl- 2H-tetrazolium bromide metabolic activity assay. It relies on the cleavage of the tetrazolium salt by mitochondrial dehydrogenases in viable cells giving the purple-colored precipitate of formazan [85], after cell incubation with the different test formulations. The medium was taken away after centrifugation at 1800 rpm for 15 minutes. Resuspended of each pellet in MTT solution 5mg/10 ml Dulbecco's modified eagle's medium (DMEM) occurred. After incubation for 3 hours at 37°C in the dark, centrifugation at 1800 rpm was performed and the supernatant in each tube rejected. Thereafter, the precipitated formazan crystals resulting from MTT conversion by mitochondrial enzymes in viable cells was dissolved in 100 µl dimethyl sulfoxide (DMSO) with the aid of a shaker for 10 minutes. Measurement of the absorbance of the resulting solution was done by a Bio-Rad microplate reader at 570 nm. All experiments were conducted in triplicate. Then, IC_{50} value of the test formulations was measured. The relative cell viability was defined as the mean percentage of viable cells compared to control untreated cells. The half maximal growth inhibitory concentrations (IC_{50}) of the test formulations were calculated by the equation.

$$\text{Viability \%} = \frac{Average\ absorbance\ (OD)\ test}{Average\ Absorbance\ (OD)\ control} x100$$

4.2.2.4. Selectivity index calculation

The selectivity index (SI) was calculated by dividing IC_{50} value by the MIC. The compound is considered to be safe if the SI is ≥ 10.

4.3. Bioactivity profiling and molecular modeling

4.3.1. Shape-based similarity

We performed shape-based similarity screening using ChemMine tools similarity workbench [86]. Compounds were fed in the form of smiles and atom pair (AP) tanimoto coefficients were automatically generated.

4.3.2. Generation of the pharmacophore model

All compounds were drawn using the Builder module of the MOE version 2016.0802 program. Energy minimization using MMFF94X force field was applied. The most active 6 compounds in the study (**8a-d, 14b** and **18**) were used as training set. The pharmacophore model was then obtained using the Unified scheme and As-Is Unique conformations field present in the Pharmacophore Elucidation module. It was then tested by mapping six compounds (**C** – **H**) on the pharmacophore model using the Pharmacophore Search module and the conformer having the lowest RMSD value was selected.

4.3.3. Inverse docking study

Computer-assisted simulated inverse docking experiment was conducted using Molecular Operating Environment (MOE 2016.0802) software, Chemical Computing Group, Montreal, Canada [71]. The docking study was performed on six active compounds (**8a-d, 14b** and **18**) against five *Mtb* target proteins.

4.3.3.1. Preparation of the proteins' crystal structures

The 3D crystal structures for DprE1 (PDB ID: **4FDO**), pantothenate synthetase (PDB ID: **3IVX**), FabH (PDB ID: **1U6S**), InhA (PDB ID: **4TZK**) and isocitrate lyase (PDB ID: **1F8M**) were retrieved from the Protein Data Bank website [87] and handled consequently with MOE program. Redundant chains, water molecules and any surfactants were discarded. Explicit hydrogen atoms were added to the receptor complex structure and partial charges were calculated. The preparation was completed with "structure preparation" module employing "protonate 3D" function. The co-crystal ligands were extracted from their corresponding proteins and used as reference molecules for the validation study.

4.3.3.2. Preparation of the ligands for docking

The target compounds were constructed using the Builder module of MOE. They were then collected in a database and prepared by adding hydrogens, calculating partial charges and energy minimizing using Force Field MMFF94x.

4.3.3.4. Docking procedure

Ligands were docked within each active site using the MOE-Dock. We used Triangle Matcher as placements method, London dG as the main scoring function. An additional refinement step using rigid receptor method with GBVI/WSA dG scoring function was also employed. Each resulted database contained the energy score between the ligands' conformers and the enzyme binding sites in kcal/mol. All receptor-ligand complexes were further investigated to examine the binding interactions to select the best docked pose. The best docked complex assumed to represent the protein-ligand interactions, was selected based on docking score, the orientation of the ligands at the active site in a similar manner to reference ligands and preservation of the key interactions. This docking approach was validated by successful pose-retrieval of the co-crystal ligand when docked into its corresponding binding site of the crystal structure. All graphical representations were rendered by MOE.2016.0802.

4.4. *In silico* prediction of drug-likeness, physicochemical properties and pharmacokinetic profile

Compounds (**8a**-**d** and **18**) were subjected to physicochemical properties prediction using Data Warrior software from Osiris property explorer. Pre-ADMET calculator was used to calculate ADME properties of the active compounds.

5. Declaration of interest

The authors report no conflicts of interest. The authors alone are responsible for the contents and writing the paper.

6.References

[1] G. Riccardi, M. Pasca, S. Buroni, Mycobacterium tuberculosis: drug resistance and future perspectives, Future Microbiol. 4(5) (2009) 597-614.

[2] B. Mathew, S. Srivastava, L.J. Ross, W.J. Suling, E.L. White, L.K. Woolhiser, A.J. Lenaerts, R.C. Reynolds, Novel pyridopyrazine and pyrimidothiazine derivatives as FtsZ inhibitors, Bioorg. Med. Chem. 19(23) (2011) 7120-7128.

[3] Global Tuberculosis Report, World Health Organization, 2018.

[4] A. Nusrath Unissa, L.E. Hanna, S. Swaminathan, A Note on Derivatives of Isoniazid, Rifampicin, and Pyrazinamide Showing Activity Against Resistant Mycobacterium tuberculosis, Chem. Biol. Drug. Des. 87(4) (2016) 537-550.

[5] L. D'Ambrosio, R. Centis, G. Sotgiu, E. Pontali, A. Spanevello, G.B. Migliori, New anti-tuberculosis drugs and regimens: 2015 update, ERJ Open Res. 1(1) (2015) 1-15.

[6] A. Koul, E. Arnoult, N. Lounis, J. Guillemont, K. Andries, The challenge of new drug discovery for tuberculosis, Nature 469(7331) (2011) 483-490.

[7] M.I. Siddiqi, A. Kumar, Review of knowledge for rational design and identification of anti-tubercular compounds, Expert Opin. Drug. Discov. 4(10) (2009) 1005-1015.

[8] A.L. Candéa, M.L. Ferreira, K.C. Pais, L.N. Cardoso, C.R. Kaiser, M.G. Henriques, M.C. Lourenço, F.A. Bezerra, M.V. de Souza, Synthesis and antitubercular activity of 7-chloro-4-quinolinylhydrazones derivatives, Bioorg. Med. Chem. Lett. 19(22) (2009) 6272-6274.

[9] Y.M. Lin, Y. Zhou, M.T. Flavin, L.M. Zhou, W. Nie, F.C. Chen, Chalcones and flavonoids as anti-Tuberculosis agents, Bioorg. Med. Chem. 10(8) (2002) 2795-2802.

[10] Y. Zhang, M.M. Wade, A. Scorpio, H. Zhang, Z. Sun, Mode of action of pyrazinamide: disruption of Mycobacterium tuberculosis membrane transport and energetics by pyrazinoic acid, J. Antimicrob. Chemother. 52(5) (2003) 790-795.

[11] Y. Zhang, Persistent and dormant tubercle bacilli and latent tuberculosis, Front. Biosci. 9(439) (2004) 1136-1156.

[12] D.A. Mitchison, The action of anti-tuberculosis drugs in short-course chemotherapy, Tubercle 66(3) (1985) 219-225.

[13] R. Shi, N. Itagaki, I. Sugawara, Overview of anti-tuberculosis (TB) drugs and their resistance mechanisms, Mini-Rev. Med. Chem. 7(11) (2007) 1177-1185.

[14] M.H. Cynamon, S.P. Klemens, T.S. Chou, R.H. Gimi, J.T. Welch, Antimycobacterial activity of a series of pyrazinoic acid esters, J. Med. Chem. 35(7) (1992) 1212-1215.

[15] M.H. Cynamon, R.H. Gimi, F. Gyenes, C.A. Sharpe, K.E. Bergmann, H.J. Han, L.B. Gregor, R. Rapolu, G. Luciano, J.T. Welch, Pyrazinoic acid esters with broad spectrum in vitro antimycobacterial activity, J. Med. Chem. 38(20) (1995) 3902-3907.

[16] O. Zimhony, J.S. Cox, J.T. Welch, W.R. Jacobs Jr, Pyrazinamide inhibits the eukaryotic-like fatty acid synthetase I (FASI) of Mycobacterium tuberculosis, Nature Medicine 6(9) (2000) 1043-1047.

[17] W. Shi, X. Zhang, X. Jiang, H. Yuan, J.S. Lee, C.E. Barry, H. Wang, W. Zhang, Y. Zhang, Pyrazinamide inhibits trans-translation in Mycobacterium tuberculosis, Science 333(6049) (2011) 1630-1632.

[18] H.I. Boshoff, V. Mizrahi, C.E. Barry, Effects of pyrazinamide on fatty acid synthesis by whole mycobacterial cells and purified fatty acid synthase I, J. Bacteriol. 184(8) (2002) 2167-2172.

[19] N.A. Dillon, N.D. Peterson, H.A. Feaga, K.C. Keiler, A.D. Baughn, Anti-tubercular Activity of Pyrazinamide is Independent of trans-Translation and RpsA, Sci. rep. 7(1) (2017) 6135.

[20] H. Kim, K. Shibayama, E. Rimbara, S. Mori, Biochemical characterization of quinolinic acid phosphoribosyltransferase from Mycobacterium tuberculosis H37Rv and inhibition of its activity by pyrazinamide, PLoS One 9(6) (2014) e100062.

[21] W. Shi, J. Chen, J. Feng, P. Cui, S. Zhang, X. Weng, W. Zhang, Y. Zhang, Aspartate decarboxylase (PanD) as a new target of pyrazinamide in Mycobacterium tuberculosis, Emerg. Microbes Infect. 3(1) (2014) 1-8.

[22] M. Njire, N. Wang, B. Wang, Y. Tan, X. Cai, Y. Liu, J. Mugweru, J. Guo, H.A. Hameed, S. Tan, Pyrazinoic acid inhibits a bifunctional enzyme in Mycobacterium tuberculosis, Antimicrob. Agents. Chemother. 61(7) (2017) e00070-17.

[23] P. Gopal, M. Yee, J. Sarathy, J.L. Low, J.P. Sarathy, F. Kaya, V. Dartois, M. Gengenbacher, T. Dick, Pyrazinamide resistance is caused by two distinct mechanisms: prevention of coenzyme A depletion and loss of virulence factor synthesis, ACS Infect. Dis. 2(9) (2016) 616-626.

[24] P. Gopal, R. Tasneen, M. Yee, J.-P. Lanoix, J. Sarathy, G. Rasic, L. Li, V.r. Dartois, E. Nuermberger, T. Dick, In vivo-selected pyrazinoic acid-resistant Mycobacterium tuberculosis strains harbor missense mutations in the aspartate decarboxylase PanD and the unfoldase ClpC1, ACS Infect. Dis. 3(7) (2017) 492-501.

[25] Y. Zhang, A. Scorpio, H. Nikaido, Z. Sun, Role of acid pH and deficient efflux of pyrazinoic acid in unique susceptibility of Mycobacterium tuberculosis to pyrazinamide, J. Bacteriol. 181(7) (1999) 2044-2049.

[26] P. Gopal, J. Sarathy, M. Yee, P. Ragunathan, J. Shin, S. Bhushan, J. Zhu, T. Akopian, O. Kandror, T.K. Lim, Pyrazinamide triggers degradation of its target aspartate decarboxylase, bioRxiv (2019) 674416.

[27] P. Gopal, G. Grüber, V. Dartois, T. Dick, Pharmacological and Molecular Mechanisms Behind the Sterilizing Activity of Pyrazinamide, Trends pharmacol sci. (2019).

[28] C.H. Lima, M.G. Henriques, A.L. Candea, M.C. Lourenco, F.A. Bezerra, M.L. Ferreira, C.R. Kaiser, M.V. de Souza, Synthesis and antimycobacterial evaluation of N'-(E)-heteroaromaticpyrazine-2-carbohydrazide derivatives, Med. Chem. 7(3) (2011) 245-249.

[29] F.M. Vergara, C.H. Lima, M.G. Henriques, A.L. Candéa, M.C. Lourenço, M.L. Ferreira, C.R. Kaiser, M.V. de Souza, Synthesis and antimycobacterial activity of N′-[(E)-(monosubstituted-benzylidene)]-2-pyrazinecarbohydrazide derivatives, Eur. J. Med. Chem. 44(12) (2009) 4954-4959.

[30] M. Kucerova-Chlupacova, J. Kunes, V. Buchta, M. Vejsova, V. Opletalova, Novel pyrazine analogs of chalcones: Synthesis and evaluation of their antifungal and antimycobacterial activity, Molecules 20(1) (2015) 1104-1117.

[31] Kucerova-Chlupacova M, Vyskovska-Tyllova V, Richterova-Finkova L, Kunes J, Buchta V, Vejsova M, Paterova P, Semelkova L, Jandourek O, O. V., Novel halogenated pyrazine-based chalcones as potential antimicrobial drugs, Molecules 21(11) (2016) 1-16.

[32] M.H. Gezginci, A.R. Martin, S.G. Franzblau, Antimycobacterial activity of substituted isosteres of pyridine-and pyrazinecarboxylic acids, J. Med. Chem. 44(10) (2001) 1560-1563.

[33] R. Maccari, R. Ottana, M.G. Vigorita, In vitro advanced antimycobacterial screening of isoniazid-related hydrazones, hydrazides and cyanoboranes: Part 14, Bioorg. Med. Chem. Lett. 15(10) (2005) 2509-2513.

[34] K. Bedıa, S. Ünsalan, S.G. Küçüzel, G. Şener, S. Rollas, HPLC analysis of in vivo metabolites of 4-nitrobenzoic acid [(5-nitro-2-thiopheneyl) methylene] hydrazide in rats, Eur. J. Drug Metab. Pharmacokinet. 32(4) (2007) 197-203.

[35] K. Bedia, O. Elçin, U. Seda, K. Fatma, S. Nathaly, R. Sevim, A. Dimoglo, Synthesis and characterization of novel hydrazide–hydrazones and the study of their structure–antituberculosis activity, Eur. J. Med. Chem. 41(11) (2006) 1253-1261.

[36] R. Kuhn, H.R. Hensel, Über 2-Aza-chalkone, Eur. J. Inorg. Chem. 86(10) (1953) 1333-1341.

[37] S.D. Joshi, S.R. Dixit, M.N. Kirankumar, T.M. Aminabhavi, K.V. Raju, R. Narayan, C. Lherbet, K.S. Yang, Synthesis, antimycobacterial screening and ligand-based molecular docking studies on novel pyrrole derivatives bearing pyrazoline, isoxazole and phenyl thiourea moieties, Eur. J. Med. Chem. 107 (2016) 133-152.

[38] N.S. Rao, A.B. Shaik, S.R. Routhu, S.M.A. Hussaini, S. Sunkari, A.V.S. Rao, A.M. Reddy, A. Alarifi, A. Kamal, New quinoline linked chalcone and pyrazoline conjugates: Molecular properties prediction, antimicrobial and antitubercular activities, Chemistry Select 2(10) (2017) 2989-2996.

[39] P.S. Shirude, B. Paul, N. Roy Choudhury, C. Kedari, B. Bandodkar, B.G. Ugarkar, Quinolinyl pyrimidines: potent inhibitors of NDH-2 as a novel class of anti-TB agents, ACS Med. Chem. Lett. 3(9) (2012) 736-740.

[40] F. Lentz, M. Hemmer, N. Reiling, A. Hilgeroth, Discovery of novel N-phenyl 1, 4-dihydropyridines with a dual mode of antimycobacterial activity, Bioorg. Med. Chem. Lett. 26(24) (2016) 5896-5898.

[41] H. Van Hattum, H. Waldmann, Biology-oriented synthesis: harnessing the power of evolution, J. Am. Chem. Soc. 136(34) (2014) 11853-11859.

[42] W.R. Galloway, A. Isidro-Llobet, D.R. Spring, Diversity-oriented synthesis as a tool for the discovery of novel biologically active small molecules, Nat. Commun. 1 (2010) 80.

[43] V. Opletalová, A. Patel, M. Boulton, A. Dundrová, E. Lacinová, M. Převorová, M. Appeltauerová, M. Coufalová, 5-Alkyl-2-pyrazinecarboxamides, 5-alkyl-2-pyrazinecarbonitriles and 5-alkyl-2-acetylpyrazines as synthetic intermediates for antiinflammatory agents, Collect. Czech. Chem. Commun. 61(7) (1996) 1093-1101.

[44] D.L. Roberts, Process of imparting a popcorn-like flavor and aroma to foodstuffs and tobacco by incorporating pyrazine derivatives therein and the resulting products, Google Patents, US, 1968.

[45] M.M. Abdel-Aziz, H.M. Abdel-Rahman, Synthesis and anti-mycobacterial evaluation of some pyrazine-2-carboxylic acid hydrazide derivatives, Eur. J. Med. Chem. 45(8) (2010) 3384-3388.

[46] J. Easmon, G. Heinisch, J. Hofmann, T. Langer, H. Grunicke, J. Fink, G. Pürstinger, Thiazolyl and benzothiazolyl hydrazones derived from α-(N)-acetylpyridines and diazines: synthesis, antiproliferative activity and CoMFA studies, Eur. J. Med. Chem. 32(5) (1997) 397-408.

[47] G.J. Karabatsos, R.A. Taller, Structural studies by nuclear magnetic resonance. V. Phenylhydrazones, J. Am. Chem. Soc. 85(22) (1963) 3624-3629.

[48] S.A. El-Hawash, A.E. Abdel Wahab, M.A. El-Demellawy, Cyanoacetic acid hydrazones of 3-(and 4-)acetylpyridine and some derived ring systems as potential antitumor and anti-HCV agents, Arch. Pharm. 339(1) (2006) 14-23.

[49] P.A. Elzahhar, S. Elkazaz, R. Soliman, A.A. El-Tombary, H.A. Shaltout, I.M. El-Ashmawy, A.E. Abdel Wahab, S.A. El-Hawash, Design and synthesis of some new 2, 3′-bipyridine-5-carbonitriles as potential anti-inflammatory/antimicrobial agents, Future Med. Chem. 9(12) (2017) 1413-1450.

[50] E. Hernandez-Nunez, H. Tlahuext, R. Moo-Puc, H. Torres-Gomez, R. Reyes-Martinez, R. Cedillo-Rivera, C. Nava-Zuazo, G. Navarrete-Vazquez, Synthesis and in vitro trichomonicidal, giardicidal and amebicidal activity of N-acetamide(sulfonamide)-2-methyl-4-nitro-1H-imidazoles, Eur. J. Med. Chem. 44(7) (2009) 2975-84.

[51] A. Geronikaki, D. Druzhilovsky, A. Zakharov, V. Poroikov, Computer-aided prediction for medicinal chemistry via the Internet, SAR QSAR Environ. Res. 19(1-2) (2008) 27-38.

[52] L. Collins, S.G. Franzblau, Microplate alamar blue assay versus BACTEC 460 system for high-throughput screening of compounds against Mycobacterium tuberculosis and Mycobacterium avium, Antimicrob. Agents. Chemother. 41(5) (1997) 1004-1009.

[53] N. Boechat, V.F. Ferreira, S.B. Ferreira, M.L. Ferreira, F.C. da Silva, M.M. Bastos, M.d.S. Costa, M.C.S. Lourenço, A.C. Pinto, A.U. Krettli, Novel 1, 2, 3-triazole derivatives for use against Mycobacterium tuberculosis H37Rv (ATCC 27294) strain, J. Med. Chem. 54(17) (2011) 5988-5999.

[54] J. Zitko, B. Servusová, P. Paterová, J. Mandíková, V. Kubíček, R. Kučera, V. Hrabcová, J. Kuneš, O. Soukup, M. Doležal, Synthesis, antimycobacterial activity and in vitro cytotoxicity of 5-chloro-N-phenylpyrazine-2-carboxamides, Molecules 18(12) (2013) 14807-14825.

[55] E.C. Hett, E.J. Rubin, Bacterial growth and cell division: A mycobacterial perspective, Microbiol. Mol. Biol. Rev. 72(1) (2008) 126-156.

[56] T. Mosmann, Rapid colorimetric assay for cellular growth and survival: application to proliferation and cytotoxicity assays, J. Immunol. Methods 65(1-2) (1983) 55-63.

[57] I. Orme, Search for new drugs for treatment of tuberculosis, Antimicrob. Agents. Chemother. 45(7) (2001) 1943-1946.

[58] T.W. Backman, Y. Cao, T. Girke, ChemMine tools: an online service for analyzing and clustering small molecules, Nucleic Acids Res. 39(suppl_2) (2011) W486-W491.

[59] K. Raman, K. Yeturu, N. Chandra, TargetTB: A target identification pipeline for Mycobacterium tuberculosis through an interactome, reactome and genome-scale structural analysis, BMC Syst. Biol. 2(1) (2008) 1-21.

[60] S.C. Ngo, O. Zimhony, W.J. Chung, H. Sayahi, W.R. Jacobs Jr, J.T. Welch, Inhibition of isolated Mycobacterium tuberculosis fatty acid synthase I by pyrazinamide analogs, Antimicrob. Agents. Chemother. 51(7) (2007) 2430-2435.

[61] S. Cole, R. Brosch, J. Parkhill, T. Garnier, C. Churcher, D. Harris, S. Gordon, K. Eiglmeier, S. Gas, C. Barry, Deciphering the biology of Mycobacterium tuberculosis from the complete genome sequence, Nature 393(6685) (1998) 537-544.

[62] J. Yang, Y. Liu, J. Bi, Q. Cai, X. Liao, W. Li, C. Guo, Q. Zhang, T. Lin, Y. Zhao, H. Wang, J. Liu, X. Zhang, D. Lin, Structural basis for targeting the ribosomal protein S1 of Mycobacterium tuberculosis by pyrazinamide, Mol. Microbiol. 95(5) (2015) 791-803.

[63] G. Riccardi, M.R. Pasca, L.R. Chiarelli, G. Manina, A. Mattevi, C. Binda, The DprE1 enzyme, one of the most vulnerable targets of Mycobacterium tuberculosis, Appl. Microbiol. Biotechnol. 97(20) (2013) 8841-8848.

[64] D. Sriram, P. Yogeeswari, D.R.K. Vyas, P. Senthilkumar, P. Bhat, M. Srividya, 5-Nitro-2-furoic acid hydrazones: design, synthesis and in vitro antimycobacterial evaluation against log and starved phase cultures, Bioorg. Med. Chem. Lett. 20(15) (2010) 4313-4316.

[65] M. Krátký, J. Vinšová, E. Novotná, J. Stolaříková, Salicylanilide pyrazinoates inhibit in vitro multidrug-resistant Mycobacterium tuberculosis strains, atypical mycobacteria and isocitrate lyase, Eur. J. Pharm. Sci. 53 (2014) 1-9.

[66] L. Semelková, P. Janošcová, C. Fernandes, G. Bouz, O. Janďourek, K. Konečná, P. Paterová, L. Navrátilová, J. Kuneš, M. Doležal, Design, synthesis, antimycobacterial evaluation, and in silico studies of 3-(phenylcarbamoyl)-pyrazine-2-carboxylic acids, Molecules 22(9) (2017) 1491.

[67] O. Jandourek, M. Tauchman, P. Paterova, K. Konecna, L. Navratilova, V. Kubicek, O. Holas, J. Zitko, M. Dolezal, Synthesis of Novel Pyrazinamide Derivatives Based on 3-Chloropyrazine-2-carboxamide and Their Antimicrobial Evaluation, Molecules 22(2) (2017) 223.

[68] J. Zitko, O. Jand'ourek, P. Paterová, L. Navrátilová, J. Kuneš, J. Vinšová, M. Doležal, Design, synthesis and antimycobacterial activity of hybrid molecules combining pyrazinamide with a 4-phenylthiazol-2-amine scaffold, MedChemComm 9(4) (2018) 685-696.

[69] P.B. Devi, S. Jogula, A.P. Reddy, S. Saxena, J.P. Sridevi, D. Sriram, P. Yogeeswari, Design of novel Mycobacterium tuberculosis pantothenate synthetase inhibitors: Virtual screening, synthesis and in vitro biological activities, Mol. Inform. 34(2-3) (2015) 147-159.

[70] T. Chitre, K. Asgaonkar, P. Miniyar, A. Dharme, M. Arkile, A. Yeware, D. Sarkar, V. Khedkar, P. Jha, Synthesis and docking studies of pyrazine–thiazolidinone hybrid scaffold targeting dormant tuberculosis, Bioorg. Med. Chem. Lett. 26(9) (2016) 2224-2228.

[71] Molecular Operating Environment. https://www.chemcomp.com/.

[72] P.S. Kharkar, S. Warrier, R.S. Gaud, Reverse docking: a powerful tool for drug repositioning and drug rescue, Future Med. Chem. 6(3) (2014) 333-342.

[73] Y. Wang, J. Xing, Y. Xu, N. Zhou, J. Peng, Z. Xiong, X. Liu, X. Luo, C. Luo, K. Chen, In silico ADME/T modelling for rational drug design, Q. Rev. Biophys. 48(4) (2015) 488-515.

[74] T. Sander, J. Freyss, M. von Korff, C. Rufener, DataWarrior: an open-source program for chemistry aware data visualization and analysis, J. Chem. Inf. Model. 55(2) (2015) 460-473.

[75] M.J. Ahsan, J. Govindasamy, H. Khalilullah, G. Mohan, J.P. Stables, C. Pannecouque, E. De Clercq, POMA analyses as new efficient bioinformatics' platform to predict and optimise bioactivity of synthesized 3a, 4-dihydro-3H-indeno [1, 2-c] pyrazole-2-carboxamide/carbothioamide analogues, Bioorg. Med. Chem. Lett. 22(23) (2012) 7029-7035.

[76] M.A. Bakht, M.S. Yar, S.G. Abdel-Hamid, S.I. Al Qasoumi, A. Samad, Molecular properties prediction, synthesis and antimicrobial activity of some newer oxadiazole derivatives, Eur. J. Med. Chem. 45(12) (2010) 5862-5869.

[77] Pre-ADMET Calculator. https://preadmet.bmdrc.kr/.

[78] H. Gainer, Notes.Synthesis of Pyrazinoic Acid, J. Org. Chem. 24(5) (1959) 691.

[79] K. Kandasamy, M.P. Pachamuthu, M. Muthusamy, S. Ganesabaskaran, A. Ramanathan, Synthesis of novel pyrazolylbiscoumarin derivatives using FeTUD-1 as a mesoporous solid acid catalyst, RSC Adv. 3(47) (2013) 25367-25373.

[80] S. Nag, V. Singh, S. Batra, Studies on the Baylis-Hillman reaction of pyrazolecarbaldehydes under the influence of DABCO: positional effect on the reactivity of the formyl group, Arkivoc 14 (2007) 185-203.

[81] G. Sivaprasad, P.T. Perumal, V.R. Prabavathy, N. Mathivanan, Synthesis and anti-microbial activity of pyrazolylbisindoles—promising anti-fungal compounds, Bioorg. Med. Chem. Lett. 16(24) (2006) 6302-6305.

[82] A. Böyum, Isolation of mononuclear cells and granulocytes from human blood. Isolation of monuclear cells by one centrifugation, and of granulocytes by combining centrifugation and sedimentation at 1 g, Scand. J. Clin. Lab. Invest. Suppl. 97 (1968) 77-89.

[83] A. Bøyum, Isolation of lymphocytes, granulocytes and macrophages, Scand. J. Immunol. 5(s5) (1976) 9-15.

[84] W. Strober, Trypan blue exclusion test of cell viability, Curr. Protoc. immunol. (2001) A3-B.

[85] N. Horiuchi, K. Nakagawa, Y. Sasaki, K. Minato, Y. Fujiwara, K. Nezu, Y. Ohe, N. Saijo, In vitro antitumor activity of mitomycin C derivative (RM-49) and new anticancer antibiotics (FK973) against lung cancer cell lines determined by tetrazolium dye (MTT) assay, Cancer Chemother. Pharmacol. 22(3) (1988) 246-250.

[86] ChemMine tools. http://chemmine.ucr.edu/.

[87] Protein Data Bank. https://www.rcsb.org/pdb/home/home.do.

List of Schemes

Scheme 1. Synthesis of the target pyrazine-2-carbohydrazides (compounds **6a-c** and **8a-d**).

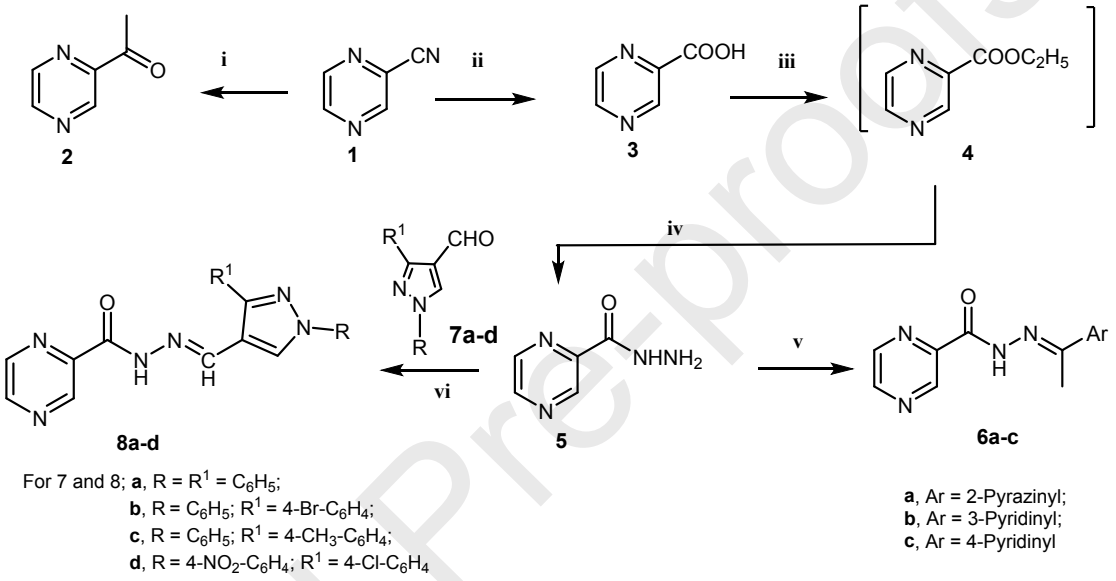

Reagents and conditions: i) 3M CH_3MgBr, dry ether, stirring at room temperature for 1h; ii) 10% NaOH, reflux for 6h; iii) H_2SO_4, EtOH, reflux for 10h; iv) $NH_2NH_2.H_2O$, EtOH, reflux for 4h; v) Ar-CHO, EtOH, reflux for 12h; vi) EtOH, reflux for 16h.

Scheme 2. Synthesis of the target carbohydrazides (compounds **10,11** and **12a-e**) and Pyrazine-pyrimidinone hybrids (compounds **13a-e**).

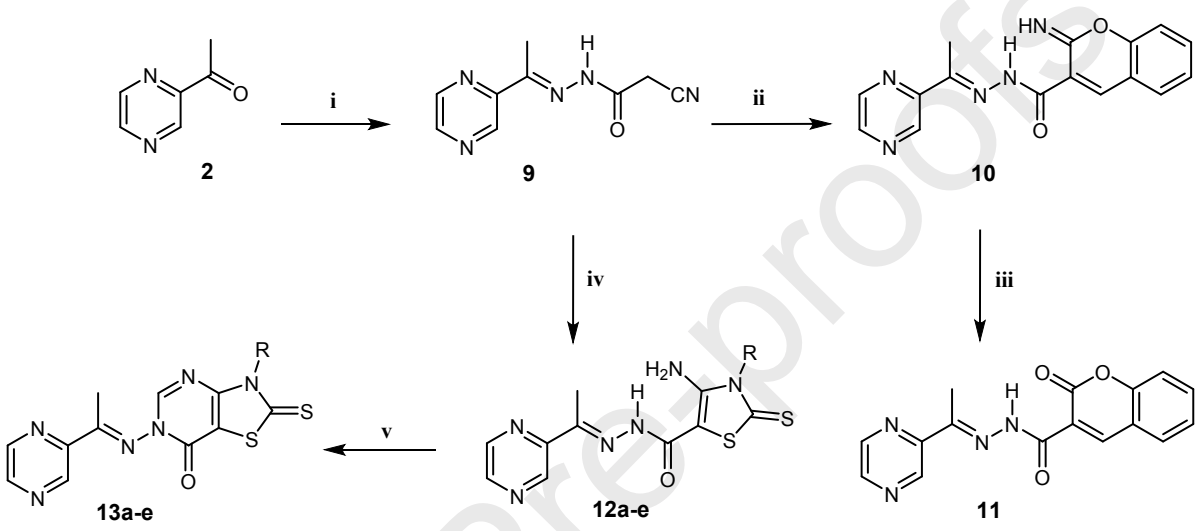

For 12 and 13: **a**, R= CH_2=CH-CH_2; **b**, R = C_6H_5; **c**, R = 4-Cl-C_6H_4; **d**, R = 4-F-C_6H_4; **e**, R =4-CH_3O-C_6H_4

Reagents and conditions: i) $NH_2NHCOCH_2CN$, EtOH, reflux for 1h; ii) salicylaldehyde, EtOH, piperidine, stirring at room temperature for 2h;
iii) EtOH, H_2O, 32% HCl (30:1:1; v/v/v), stirring at room temperature for 1h;
iv) RNCS/S, EtOH, DMF, Et_3N, reflux for 1h;
v) triethylorthoformate, Ac_2O, reflux for 3h.

Scheme 3. Synthesis of the target hybrids (compounds **14-21**)

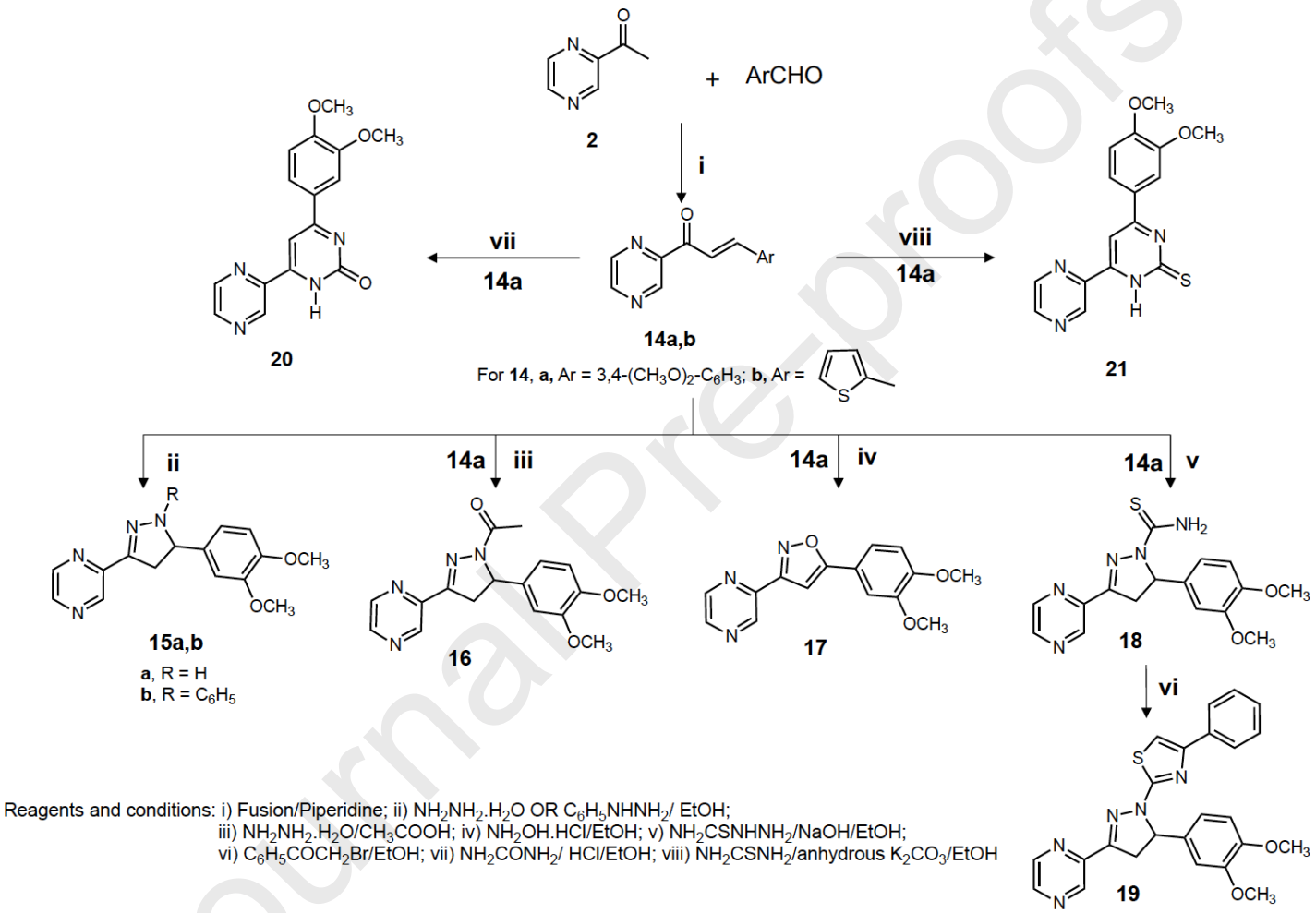

Reagents and conditions: i) Fusion/Piperidine; ii) $NH_2NH_2.H_2O$ OR $C_6H_5NHNH_2$/ EtOH;
iii) $NH_2NH_2.H_2O/CH_3COOH$; iv) $NH_2OH.HCl/EtOH$; v) $NH_2CSNHNH_2/NaOH/EtOH$;
vi) $C_6H_5COCH_2Br/EtOH$; vii) NH_2CONH_2/ HCl/EtOH; viii) NH_2CSNH_2/anhydrous K_2CO_3/EtOH

Scheme 4. Synthesis of the target hybrids (compounds **22-25**)

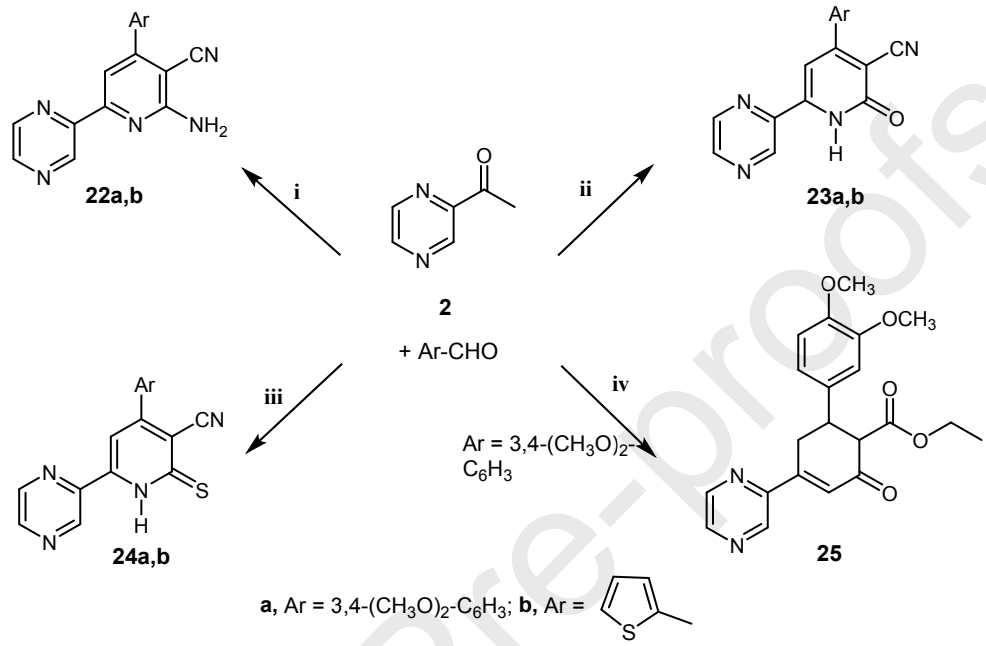

Reagents and conditions: i) $CNCH_2CN$, NH_4OAc, EtOH, reflux for 8 h; ii) $CNCH_2COOCH_2CH_3$, NH_4OAc, EtOH, reflux for 4 h; iii) $CNCH_2CSNH_2$, NH_4OAc, EtOH, reflux for 8 h; iv)$CH_3COCH_2COOCH_2CH_3$, 10% NaOH, EtOH, reflux for 6 h.

Figure Captions:

Figure 1. Reported pyrazine derivatives as anti-tubercular agents.

Figure 2. Outline for the design of the target compounds.

Figure 3. **(A)** Pharmacophore model (F1, orange spherical mesh, aromatic or Pi ring centers), (F2 and F3, green spherical meshes, hydrophobic region) and (F4, cyan spherical mesh, hydrogen bond acceptor projection). **(B)** Overlay of training set compounds (**8a-d**, **14b** and **18**) on the pharmacophore model.

Figure 4. Docking and binding pattern of compound **8b** (in orange) into pantothenate synthetase active site (PDB 3IVX) and its overlay over FG6 (in yellow) in 3D (left panel). Ligand interactions in 2D (right panel).

Figure 5. Docking and binding pattern of compound **14b** (in pink) into pantothenate synthetase active site (PDB 3IVX) and its overlay over FG6 (in yellow) in 3D (left panel). Ligand interactions in 2D (right panel).

Figure 6. Docking and binding pattern of compound **18** (in pink) into pantothenate synthetase active site (PDB 3IVX) and its overlay over FG6 (in yellow) in 3D (left panel). Ligand interactions in 2D (right panel).

Schemes Captions:

Scheme 1. Synthesis of the target pyrazine-2-carbohydrazides (compounds **6a-c** and **8a-d**).

Reagents and conditions: i) 3M CH_3MgBr, dry ether, stirring at room temperature for 1h; ii) 10% NaOH, reflux for 6h; iii) H_2SO_4, EtOH, reflux for 10h; iv) $NH_2NH_2.H_2O$, EtOH, reflux for 4h; v) Ar-CHO, EtOH, reflux for 12h; vi) EtOH, reflux for 16h.

Scheme 2. Synthesis of the target carbohydrazides (compounds **10,11** and **12a-e**) and Pyrazine-pyrimidinone hybrids (compounds **13a-e**).

Reagents and conditions: i) $NH_2NHCOCH_2CN$, EtOH, reflux for 1h; ii) salicylaldehyde, EtOH, piperidine, stirring at room temperature for 2h; iii) EtOH, H_2O, 32% HCl (30:1:1; v/v/v), stirring at room temperature for 1h; iv) RNCS/S, EtOH, DMF, Et_3N, reflux for 1h; v) triethylorthoformate, Ac_2O, reflux for 3h.

Scheme 3. Synthesis of the target hybrids (compounds **14-21**).

Reagents and conditions: i) Fusion at 85^0C for 1h, Piperidine; ii) $NH_2NH_2.H_2O$ OR $C_6H_5NHNH_2$, EtOH, reflux for 10 h; iii) $NH_2NH_2.H_2O$, CH_3COOH, reflux for 16 h; iv) $NH_2OH.HCl$, EtOH, reflux for 10 h; v) $NH_2CSNHNH_2$, NaOH, EtOH, reflux for 12 h; vi) $C_6H_5COCH_2Br$, EtOH, reflux for 6 h; vii) NH_2CONH_2, HCl, EtOH, reflux for 6 h; viii) NH_2CSNH_2, anhydrous K_2CO_3, EtOH, reflux for 12 h.

Scheme 4. Synthesis of the target hybrids (compounds **22-25**).

Reagents and conditions: i) $CNCH_2CN$, NH_4OAc, EtOH, reflux for 8 h; ii) $CNCH_2COOCH_2CH_3$, NH_4OAc, EtOH, reflux for 4 h; iii) $CNCH_2CSNH_2$, NH_4OAc, EtOH, reflux for 8 h; iv) $CH_3COCH_2COOCH_2CH_3$, 10% NaOH, EtOH, reflux for 6 h.

Research highlights:

- A new series of pyrazine derivatives were designed and synthesized as new structural candidates suitable for the development of new anti-TB agents.
- Six compounds displayed potent activity with MIC values ≤ 6.25 μg/ml.
- The most active compounds showed reasonable safety margins with selectivity indices ≥ 200.
- A three-step target fishing study postulated pantothenate synthetase as possible molecular mycobacterial target. Docking studies on the enzyme highlighted favorable interaction patterns.
- Physicochemical, ADME and drug-like properties were found to be adequate.

Graphical abstract:

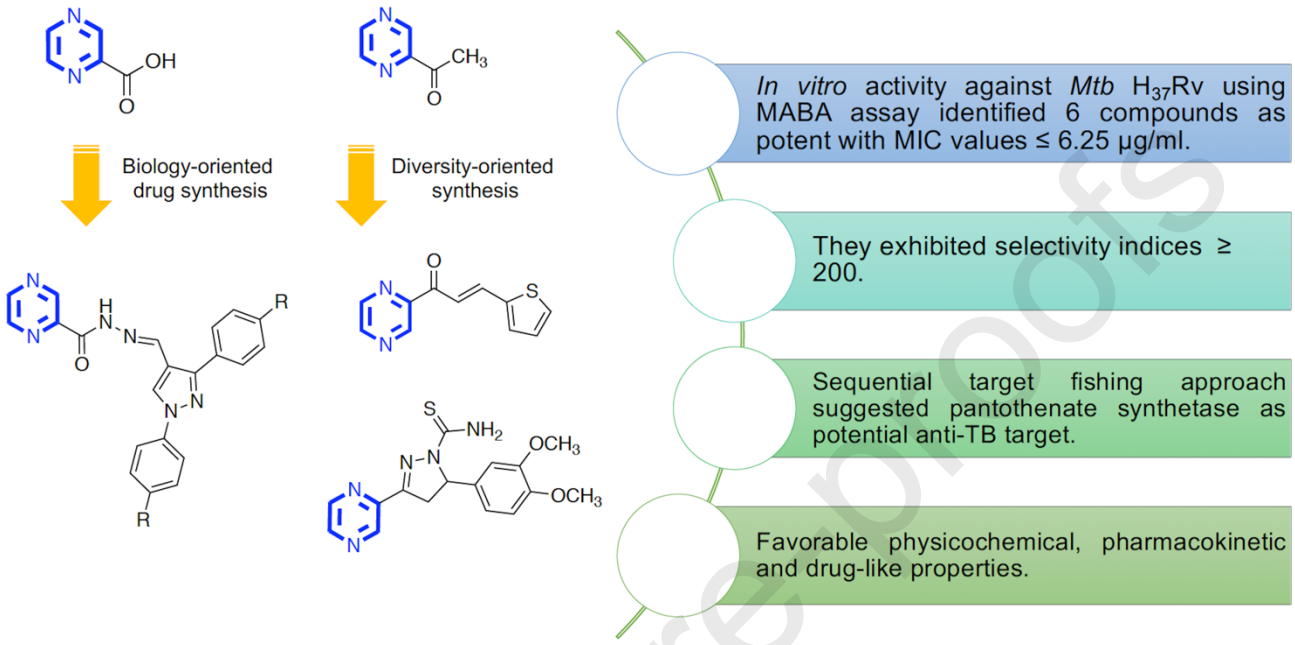

Declaration of interest

The authors report no conflicts of interest. The authors alone are responsible for the contents and writing the paper.